August 2020

The Effect of Excess Lithium on the Phase Formation, Structure and Electrical Properties of LLZO Garnet Structured Solid-State Electrolyte

Katherine Bolek
Clemson University, kbolek@g.clemson.edu

The Effect of Excess Lithium on the Phase Formation, Structure and Electrical Properties of LLZO Garnet Structured Solid-State Electrolyte

---

A Thesis
Presented to
the Graduate School of
Clemson University

In Partial Fulfillment
of the Requirements for the Degree
Master of Science
Materials Science and Engineering

---

by
Katherine Bolek
August 2020

Accepted by:
Kyle Brinkman, Committee Chair
Jianhua Tong
Ming Tang

ABSTRACT

Solid-state lithium ion batteries are currently at the forefront of investigations to replace conventional lithium ion batteries in order to improve overall safety and device performance. Researchers have investigated many substitutes to organic based conventional liquid electrolytes that result in high levels of Li ion conductivity. Cubic $Li_7La_3Zr_2O_{12}$ (LLZO) is a leader among solid-state electrolyte research. Unfortunately, pure LLZO at room temperature is generally a tetragonal structure that is significantly less conductive than cubic LLZO. This research uses a gallium dopant to reach the highly conductive cubic LLZO structure. However, a dopant is not enough to ensure a highly conductive LLZO sample. Lithium evaporates during the calcining and sintering stages of sample preparation. In order to reach an actual composition close to the targeted composition, additional lithium must be added, or lithium loss must be prevented.

The goal of this research is to investigate the best methods and amounts of excess lithium to add in order to obtain a composition as close as possible to the targeted compositions. The most common method in literature to combat lithium loss is the addition of an excess lithium precursor to the initial set of precursors. This research studied the effect of excess Li_2CO_3 precursors in LLZO at zero, ten, twenty, and thirty weight percent excess. Another method studied in this research to prevent lithium loss was using a boating technique with excess lithium carbonate. Half a gram of lithium carbonate was placed on the edges of the sintering crucible, while the sample pellets were in the middle of the crucible untouched by the excess powder. The lithium carbonate powder evaporated during sintering resulting in a build-up of lithium vapor pressure in

the crucible which will aid in lithium retention as it is more difficult to evaporate in high vapor pressure conditions.

This research found that gallium doped LLZO ($Ga_{0.5}Li_{5.5}La_3Zr_2O_{12}$) with ten weight percent excess Li_2CO_3 precursor along with the boating technique resulted in the highest density and highest conductivity of all samples tested. While more testing needs to be done on this research, the data shows how important lithium content is to produce a highly conductive solid electrolyte.

ACKNOWLEDGMENTS

I would like to extend my sincerest gratitude towards many people for getting me through the past two years of my masters and showing me that I am capable of more than I thought. First and foremost, I would like to thank Dr. Kyle Brinkman for being my advisor the past two years. Dr. Brinkman helped me navigate my research and thesis while showing patience beyond what could have been expected. I owe my newfound confidence in engineering to him. I would also like to thank Dr. Jianhua Tong and Dr. Ming Tang for serving as my advisory committee members and helping guide me towards my finished thesis.

I would like to extend a thank you to all my lab group members for assisting me in my thesis research including Nancy Birkner, Jack Duffy, Jun Gao, Robert Grote, Akihiro Ishii, Changlong Li, Yuqing Meng, and Mingyang Zhao. I would like to specifically thank my PhD mentor, Changlong Li, who was always available these past two years training, guiding, and assisting me in my research. I could not have done this without him. Nancy Birkner was also integral to my thesis process as she helped me go through numerous rounds of edits for each chapter, and I would like to thank her for all the time, effort, and guidance she put into myself and my work.

Lastly, I would like to thank my friends and family for supporting me during these last two years of school. I'd like to thank my parents specifically for always cheering me on and keeping me going throughout my masters, I would not have been able to accomplish any of this without them.

TABLE OF CONTENTS

Page

Table of Contents (Continued)

LIST OF TABLES

LIST OF FIGURES

Figure

Page

CHAPTER ONE

INTRODUCTION

1.1 Background on Solid State Batteries

Lithium ion batteries have been a reliable energy source since its invention in the 1970's. [1] However, the liquid electrolyte within lithium ion batteries present several hazards. [2], [3] The liquid electrolyte to a lithium ion battery is primarily made up of a lithium salt in an organic solvent. [4], [5] This presents the problems of dendrite formation, flammability, volatility, and instability of the liquid electrolyte. [6] All of these can contribute to the battery failure and the tendency to explode. [2], [7] These problems have presented themselves in society such as the Galaxy Note 7 or Boeing 787 incidents which exemplify the need to improve lithium ion battery safety. [8], [9]

Figure 1-1 illustrates a conventional battery and a solid-state battery. The main difference is the electrolyte between the two electrodes, a conventional battery has the liquid organic solvent immersing the two electrodes while a solid-state battery has a solid electrolyte in between the electrodes. [10] A solid electrolyte solves these problems but must be able to attain a similar ionic conductivity demonstrated in organic liquid electrolytes to produce the same amount of power as a liquid electrolyte battery. [11] Inherently, a liquid electrolyte will conduct better than a solid due to the increased mobility of a liquid as compared to that of a solid. In order to address this, solid electrolytes with a high lithium ionic conductivity of ~10^{-4} S/cm or higher are being widely researched. One of the main materials under scrutiny in this research is $Li_7La_3Zr_2O_{12}$ (LLZO).

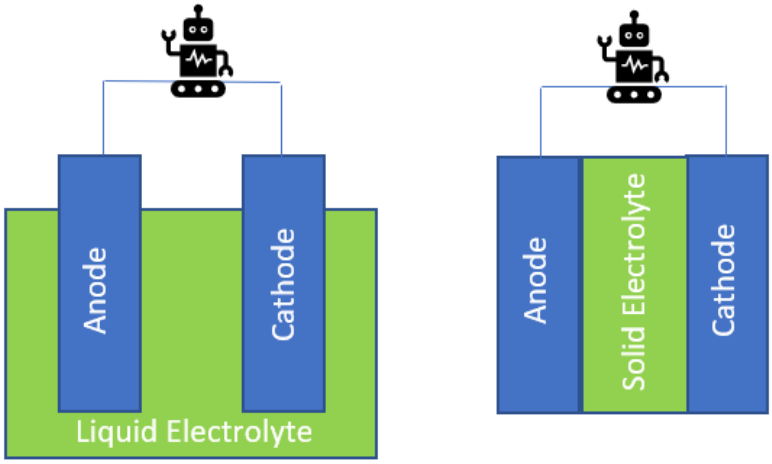

Figure 1-1 Illustrations of a conventional battery (left) and a solid-state battery (right)

1.2 LLZO Solid State Electrolyte

LLZO has been discovered as a possible solid electrolyte replacement to the liquid electrolyte. Studies show that LLZO improves the safety, reliability, and endurance of lithium ion batteries. [12], [13] One of the main difficulties with LLZO is achieving the proper phase that possesses high ionic conductivity. LLZO is generally tetragonal in its pure form which does not result in high conductivity. [14] In the cubic structure, LLZO has a much higher conductivity, however the cubic phase of LLZO is not thermodynamically stable at ambient temperature. In order to stabilize the cubic structure dopants are incorporated into the crystalline lattice.

Many dopants for LLZO have been investigated such as aluminum, gallium, niobium, gadolinium, and tantalum. [13], [15] Different dopants replace different elements within the principal lattice, replacing either lithium or zirconium. Common dopants used to target lithium and lower lithium content are aluminum, gallium, and iron. These are dopants from anions that help to replace and create vacancies in lithium sites.

In order to substitute for lithium, the molecular formula used is $Li_{7-3x}M_xLa_3Zr_2O_{12}$ where M is the dopant. [15] Gallium was tested in literature to dope LLZO with the formula $Li_{7-2X}La_3Zr_2Ga_XO_{12}$ (X=0-1). [13] The X=0.5 composition provided the best results with a room temperature conductivity of $4.37 \times 10^{-4} S/cm$. Conversely, dopants may be made of cations to substitute for the zirconium which results in the formation of lithium vacancies to balance the positive charge from the cation. [16], [17] However, when substituting for zirconium in LLZO the molecular formula used is $Li_{7-y}La_3Zr_{2-y}M_yO_{12}$ where M is the cation dopant. [18] Gadolinium, Gd^{+3} dopes the Zr^{+4} sites, producing the formula $Li_{7+X}La_3Zr_{2-X}Gd_XO_{12}$ where X=0-0.5. $Li_{7.2}La_3Zr_{1.8}Gd_{0.2}O_{12}$ achieved the highest conductivity with a room-temperature total conductivity of $2.3 \times 10^{-4} S/cm$. [19]

The proper amount of dopant and which dopant is best utilized differs among research papers. Literature has reported gallium as a viable dopant, while the amount of gallium dopant differs most use X=0.05-1.0 gallium. [13], [20], [21], [22], [23] X=0.5 gallium is used in this research as a middle ground to what previous literature has used. In this research LLZO pellets were made using pure LLZO, $Li_7La_3Zr_2O_{12}$, as a control as well as X=0.5 gallium LLZO, $Ga_{0.5}Li_{5.5}La_3Zr_2O_{12}$.

Other challenges that currently impede progress in solid state batteries are interfacial issues and the instability in air. [4], [5] Interfacial issues will always be a problem with solid electrolytes rather than liquid ones. A liquid will always have more contact with solid electrolytes because its enhanced contact with the entire surface. However, research has been performed to improve the intimate contact between solid electrolyte and solid electrode involving proper grinding and polishing to allow better

contact. [24], [25] Solid electrolytes have an instability in air after sintering where the surface of the electrolyte samples can react with the air to produce a surface layer that is non-conductive and must be removed via polishing. [5] This research placed all samples in a glovebox after sintering to ensure this reaction with air does not factor into the experimental results.

1.3 Background on Excess Lithium in LLZO

This research will revolve around the addition of excess lithium carbonate to LLZO material. Excess lithium is necessary for LLZO cubic formation due to lithium loss while sintering the material. [6], [23] Due to a high calcining/sintering temperature of 1050℃/1150℃ respectively, some lithium can evaporate, preventing the high-performance cubic phase LLZO from fully forming. Depending on the amount of excess lithium salt added to LLZO, it can cause various deviations of the stoichiometric lithium ratio which can result in differing concentrations of lithium ions and vacancies within LLZO grains. [5] These changes can in turn affect the crystal structure and ionic conductivity of LLZO.

Studies have discussed other advantages to excess lithium additions besides making up for lost lithium such as improved ionic conductivity, less interaction with aluminum crucible during calcining/sintering, and improved density of LLZO. [6] Adding excess lithium allows cubic LLZO to form easier, creating a more dense and conductive material. Many studies add 10% weight excess lithium to their mixtures. [21], [26] However, in some studies various amounts of excess lithium from 10-50% excess lithium. [6], [23], [27] It is important to note some studies use mol% while others use

weight% of excess lithium carbonate or lithium oxide. Based on known reports in literature, this research will test 10, 20, and 30% weight excess lithium carbonate for LLZO. In order to have control groups this research will also experiment with undoped LLZO and 0.5 Ga LLZO totaling to 6 different samples in this research shown in Table 1-1. LLZO and Ga-LLZO with no interior excess lithium is also researched as a control group.

Samples	
Without 0.5 grams Li_2CO_3 during sintering (boating)	With 0.5 grams Li_2CO_3 during sintering (boating)
$Li_7La_3Zr_2O_{12}$	$Li_7La_3Zr_2O_{12}$
$Li_7La_3Zr_2O_{12}$ with 10wt% excess Lithium salt	$Li_7La_3Zr_2O_{12}$ with 10wt% excess Lithium salt
$Li_7La_3Zr_2O_{12}$ with 20wt% excess Lithium salt	$Li_7La_3Zr_2O_{12}$ with 20wt% excess Lithium salt
$Li_7La_3Zr_2O_{12}$ with 30wt% excess Lithium salt	$Li_7La_3Zr_2O_{12}$ with 30wt% excess Lithium salt
$Ga_{0.5}Li_{5.5}La_3Zr_2O_{12}$	$Ga_{0.5}Li_{5.5}La_3Zr_2O_{12}$
$Ga_{0.5}Li_{5.5}La_3Zr_2O_{12}$ with 10wt% excess Lithium salt	$Ga_{0.5}Li_{5.5}La_3Zr_2O_{12}$ with 10wt% excess Lithium salt
$Ga_{0.5}Li_{5.5}La_3Zr_2O_{12}$ with 20wt% excess Lithium salt	$Ga_{0.5}Li_{5.5}La_3Zr_2O_{12}$ with 20wt% excess Lithium salt
$Ga_{0.5}Li_{5.5}La_3Zr_2O_{12}$ with 30wt% excess Lithium salt	$Ga_{0.5}Li_{5.5}La_3Zr_2O_{12}$ with 30wt% excess Lithium salt

Table 1-1 List of sample compositions in research

One thing to consider when using excess lithium is that the lithium salt can react with the aluminum crucible during the sintering process. As the temperature rises to 1150 ℃ the aluminum and lithium can react causing a minor melt phase with any alumina dissolved during the sintering process forming Li_2O-Al_2O_3 compounds. [5] Liu et al reported that increasing the amount of excess lithium enhances the interaction between lithium and alumina altering the aluminum content in the samples. [1] Liu et al concluded that as the amount of excess lithium salt increased, the Al content in sintered pellets also increased. [1] Aluminum content can affect ionic conductivity of LLZO as well meaning that the aluminum content in LLZO acts as a doping element as well as a sintering aid leading to a denser and more conductive product. This aluminum content in the samples can then alter the properties of the samples.

A highly dense conductor is better at conducting than a porous one because the air pockets prevents conduction from one side of the electrolyte sample to the other lowering the conductivity. Increasing the amount of excess lithium can increase the density of LLZO. [27], [28] Literature shows that while excess lithium is useful and necessary, too much excess lithium can lead to some challenges. Other studies have concluded that adding more than 30% excess lithium can lead to the density increase becoming smaller. [6], [13] These results led to the setup of this research by limiting the excess lithium amounts to 10-30% excess lithium salts with no excess as a control. This limitation cuts down on the variation of samples to only eight different mixtures and targets the best data based off previous research. These eight compositions are then sintered either utilizing

the boating technique or not which produces twice as many testing samples, totaling to sixteen. Table 1-2 displays all the sample types and their shorthand name.

Sample Formal Name	**Sample Shorthand**
$Li_7La_3Zr_2O_{12}$	Pure 0
$Li_7La_3Zr_2O_{12}$ with 10 wt% excess Li_2CO_3	Pure 10
$Li_7La_3Zr_2O_{12}$ with 20 wt% excess Li_2CO_3	Pure 20
$Li_7La_3Zr_2O_{12}$ with 30 wt% excess Li_2CO_3	Pure 30
$Ga_{0.5}Li_{5.5}La_3Zr_2O_{12}$	Ga-LLZO 0
$Ga_{0.5}Li_{5.5}La_3Zr_2O_{12}$ with 10 wt% excess Li_2CO_3	Ga-LLZO 10
$Ga_{0.5}Li_{5.5}La_3Zr_2O_{12}$ with 20 wt% excess Li_2CO_3	Ga-LLZO 20
$Ga_{0.5}Li_{5.5}La_3Zr_2O_{12}$ with 30 wt% excess Li_2CO_3	Ga-LLZO 30

Table 1-2 Sample shorthand names

Ionic conductivity is the main property being tested in solid state lithium ion batteries. The more conductivity a solid-state electrolyte has the better it will be at conducting ions in a battery to improve performance of the battery. Liu et al reports that as the lithium content increased closer to the targeted composition, the ionic conductivity increased significantly leveling off at approximately 4×10^{-4} S/cm. [6] In this research the only variation was the amount of excess lithium salt meaning that the difference in conductivity can be attributed to the change in density and aluminum content which all stemmed from the different amounts of excess lithium. It is also important to note that the density and ionic conductivity vary similarly as the amount of lithium carbonate is increased indicating that density and ionic conductivity are related.

Another way to mitigate the lithium loss is combatting the loss from the exterior. While preparing the pellets for sintering, 0.5 grams of Li_2CO_3 was pressed on the sides of the crucible while not touching the pellets. If the pellets and powder were to touch the Li_2CO_3 could sinter with the pellets. Instead, the goal is to have the 0.5 grams evaporate due to the high temperature creating a higher vapor pressure in the crucible forcing the lithium in the pellets to stay in and not evaporate off. This added vapor pressure should force the pellets to fully sinter with minimal lithium loss. This added pressure along with the interior addition of excess Li_2CO_3 should work together to keep the maximum amount of lithium in the pellet.

Dopants along with excess lithium help the composition reach a cubic structure enabling a higher conductivity. Regardless of which dopant is used, it will help create three lithium vacancies but only two will be shown because the dopant used fills one of these three vacancies. [18] Upon researching various dopants for LLZO gallium, aluminum, and iron were found as viable candidates because they are cations that will substitute for the Li vacancies.

Based off the current work being performed on LLZO, this research will primarily investigate how excess lithium effects LLZO as a solid-state electrolyte. Literature has shown that most experiments add ten weight percent excess lithium to their LLZO precursor mixtures, however some literature has shown the use of lithium and tested the overall conductivity. This research will take this literature a step further by investigating two methods of excess lithium addition as well as looking at an overall change in the samples rather than just conductivity. This research will make pure and gallium doped

LLZO samples and test their composition, structure, microstructure, and conductivity. This well-rounded testing will show how the excess lithium additions can alter density, grain size, targeted composition, and conductivity in order to define the ideal amount of excess lithium for LLZO solid electrolytes.

CHAPTER TWO

EXPERIMENTAL METHODS

2.1 Sample Preparation

Samples in this work were prepared utilizing a solid-state reaction method. Sample preparation begins with combining all precursor powders in a sealed container. The raw precursor powders used for LLZO were Li_2CO_3 (99.9%, Macron Fine Chemicals), La_2O_3 (99.99%, Acros Organics), and ZrO_2 (99.7%, Alfa Aesar) with the addition of Ga_2O_3 (99.99%, Aldrich) if using dopant as displayed in Table 2-1. Batches were made in sizes of ten grams for each sample type. Excess lithium was added prior to ball-milling and based on the weight percent of the initial amount of Li_2CO_3 required to make that targeted composition of LLZO. Powders were ball-milled with zirconia balls in ethanol as a dispersing reagent in a sealed container for twenty-four hours.

Sample Type	Precursor Powders
LLZO	Li_2CO_3, La_2O_3, and ZrO_2
Ga-LLZO	Ga_2O_3, Li_2CO_3, La_2O_3, and ZrO_2

Table 2-1 Precursor Powders for Sample Types

After the completion of ball-milling, the powders were left exposed to air until the ethanol evaporated. Powders were then grinded down using a mortar and pestle before being prepared for calcination. Calcination is the heating of metals below their melting temperatures, which allows for the required energy to form crystalline structures. This is considered the reaction step because this is when the Ga-LLZO samples change from

tetragonal structure to cubic structure. The pure LLZO samples will remain tetragonal after calcination but do exhibit cubic features when brought up to the transition temperatures. Literature has reported tetragonal to cubic phase transitions for pure LLZO at temperatures 100-200℃ [29], 100-150℃ [30], 200-300℃ [31], 645℃ [29], and 700-800℃ [31]. The lower temperature range phase transition is due to the hydration of the garnet structure leading to H^+/Li^+ exchange leading to a lithium defective cubic phase. [30] The pure LLZO likely reverses back to tetragonal above the low transition temperatures due to the water evaporation, this removes the H^+/Li^+ leading to the lithium reverting to their sites causing the LLZO to become tetragonal again. [31] Powders were placed into individual crucibles after grinding and were sealed closed in preparation for calcining. The crucibles were then slid into a tube furnace (Lindberg/Blue) for calcination and were heated to 950℃ for five hours. Crucibles were taken out once tube furnace was completely cooled.

The calcined powders were then ground again with a mortar and pestle to create a fine powder. While preparation is not complete yet, the powders must be X-Rayed at this point to see if the powder achieved a cubic structure during the calcining process. If the X-ray Diffraction (XRD) pattern shows a cubic structural pattern, then the powder can move on to the next step in preparation. The pure LLZO samples showed tetragonal structures in this step but continued to the next step because pure LLZO is a control and will not be cubic at room temperature with this preparation style. The calcined powders are mixed in a mortar with approximately five drops of polyvinyl acetate (PVA) to enable cold-pressing pellets. The PVA helps the powder stick together when pressed, if it were

not used the pellets would break apart prior to sintering. Once the PVA was dry and combined in the powder, the powder was cold-pressed. Approximately one gram of powder was added to the fifteen-millimeter diameter die. The samples were then cold pressed to 15,000 psi and ejected from the die.

After cold-pressing, the pellets were ready for sintering. Sintering involves heating up a powder to make it more compact and increase strength and integrity of the microstructure. The samples were put in individual crucibles with their mother powder dusted on the bottom to prevent the samples from sticking to the crucible.

If the sample was utilizing boating excess lithium, half a gram of Li_2CO_3 powder is packed to the sides of the crucible, being careful to separate the pellets from the surrounding powder so that they do not react with each other. Half a gram of lithium carbonate was chosen for the boating technique after testing boating with a gram and half gram of excess lithium carbonate. When a gram of lithium carbonate was used for boating it was too difficult to keep all the powder separated from the pellets and resulted in some of the lithium carbonate touching the pellets and reacting during the sintering process. Half a gram of lithium carbonate for boating never touched or reacted with the pellets and was therefore chosen as the amount to boat. Less lithium carbonate could have been used as well, but the goal of the powder is to provide as much lithium vapor pressure as possible in the crucible so half a gram of lithium carbonate provides the maximum that can be added without touching the pellets.

The boating method can be seen in Figure 2-1 where the powder surrounds the pellets. The goal of this method was to utilize the lithium vapor pressure from the

evaporated boating powder to essentially push the lithium into the samples and keep them from evaporating as well. The crucibles were sealed and slid into the same tube furnace used for calcining. The crucibles heat up to 1150℃ and remain at that temperature for five hours before being cooled down in the tube furnace at a heating/cooling rate of 5 degrees per minute. 1150℃ was found to be adequate temperature for sintering based off of other literature. [32], [33] Once the crucibles were completely cooled, they were removed from the tube furnace.

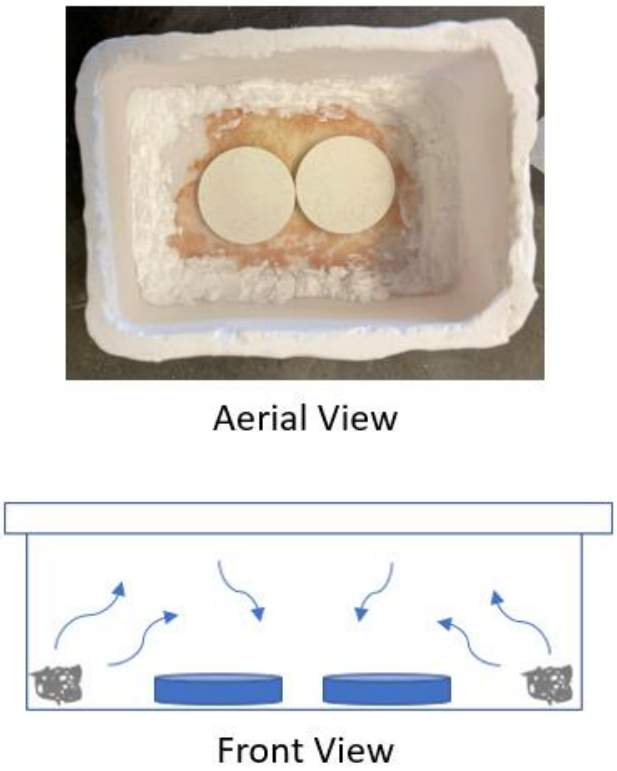

Figure 2-1 Boating excess lithium process

The sintered pellets then were ground and polished using a polishing wheel. All sample pellets were ground and polished the same way beginning with a 600-grit sanding disc (Finish 1st), then a 1200-grit sanding disk (Finish 1st), and finally polished with a

2000-grit disk (Finish 1st). At this point, samples were ready for characterization. Characterization tests included X-Ray diffraction (XRD), scanning electron microscopy (SEM), and Archimedes and geometrical density. After characterization tests concluded, the samples performed electrochemical impedance spectroscopy (EIS) testing.

2.2 Characterization Techniques

LLZO pellets must be characterized in order to see if the targeted composition was met, the crystal system of the samples, and the overall conductivity. In order to get this overall characteristic view of the samples, X-Ray diffraction (XRD), scanning electron microscopy (SEM), density, and electrochemical impedance spectroscopy (EIS) testing must be done.

2.2.1 X-Ray Diffraction

X-Ray diffraction uses x-rays to get a clear image of the elements and compounds of a material. [34] This research utilizes a Rigaku Ultima IV diffractometer to test the calcined powders and sintered pellets. The diffractometer sends an incident x-ray through a copper sealed tube at an incident angle, θ_I, towards the pellet. [35] This x-ray diffracts from the sample into a detector as shown in Figure 2-2. This beam tells us what elements are in the sample based off the angle, 2θ, it diffracts off the sample and into the detector. The incident angle then changes, and more x-rays are sent through, it is important to test many incident angles so there is a clear view of all possible angles and d-spacing. [35]

The Rigaku Ultima IV works best with samples in powder form, the pellets were ground to a powder for x-ray testing. Samples were tested from 15-50 degrees at a scan

rate of one degree per minute. The Rigaku diffractometer is capable of investigating phase identification, crystallinity, and particle size evaluations. [36] In this research is it primarily used for phase identification and crystallinity. The x-ray diffraction pattern will tell us if any secondary phases are present and whether the system is cubic or tetragonal. LLZO is only a useful electrolyte when it is cubic with no secondary phases.

All reference patterns used in this research were found at https://pubs.acs.org/ free of charge.

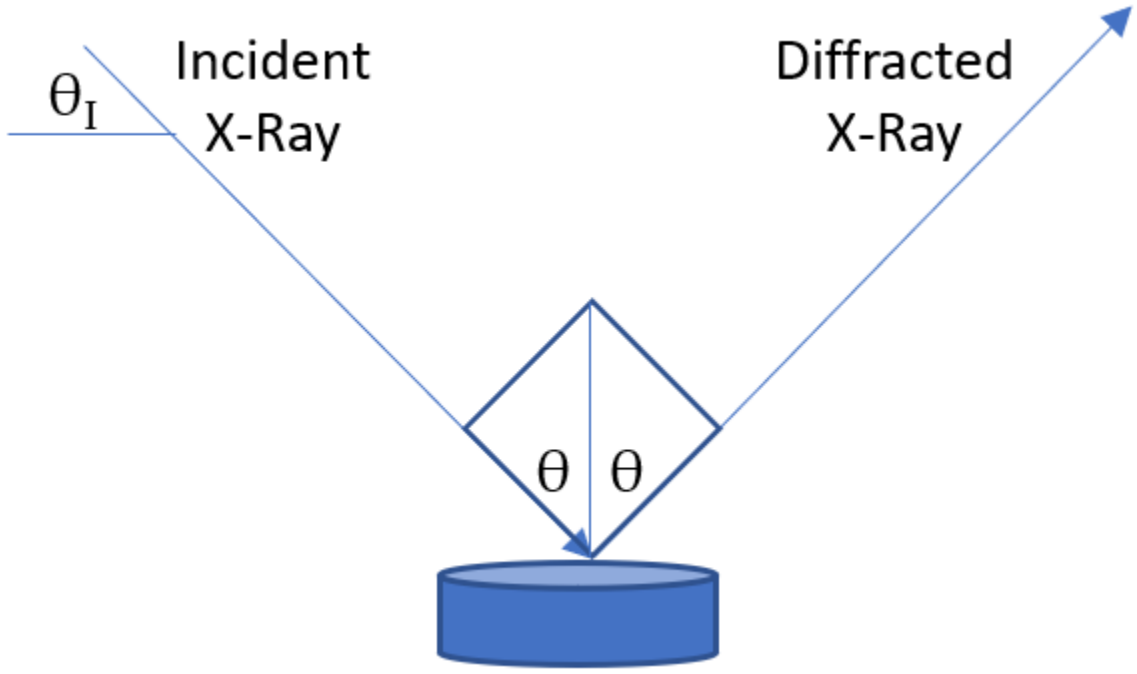

Figure 2-2 Illustration of x-ray diffraction process

2.2.2 Scanning Electron Microscopy

Scanning electron microscopy, SEM, is a vital test used in materials science. SEM produces a magnified picture of a sample far more microscopic than the naked eye or a basic microscope. [37] SEM sends electrons from a beam and have the electrons hit the

sample and bounce off into a detector. [38] Based on the angle that the electrons bounce off tells the microscope how the sample looks producing a microscopic image of the sample. [39] This research uses a Hitachi S6600 microscope which is capable of scanning electron microscopy (SEM) and energy-dispersive x-rays (EDX).

EDX is useful because it generates information about the chemical composition as well as the how the elements are distributed and concentrated throughout a sample. [40] EDX still uses the Hitachi S6600 but uses the electrons differently. The electrons hit the sample and kick an electron from the inner shell of an atom on the sample. This will leave a electron hole in its place which attracts an outer shell electron to replace the hole. When the outer shell electron jumps to the inner shell, the energy difference releases an x-ray which is then detected. [41] The x-rays all correspond to specific elements and transition to give a map of what elements are where on the sample and what concentration they are in. [42] EDX is often used to compare elemental concentrations with inductively coupled plasma mass spectrometry (ICP-MS) data to compare the results. While EDX is useful it does not pick up all elements, unfortunately lithium is too light of an element to be picked up by EDX on the Hitachi S6600. This is because lithium is such a light element it often emits an auger electron, rather than a photon, which will not be picked up by the EDX. [43] Due to this discrepancy samples were sent to Savannah River National Lab research facility for ICP-MS analysis comparison because ICP-MS is sensitive enough to detect lithium concentration. [44], [45] Savannah River National Lab used a Agilent 7500s ICP-MS for testing. The EDX data shows lanthanum, zirconium, and oxygen concentrations to compare to the ICP-MS.

SEM shows a clear microscopic image of samples so that grain size and shape can be characterized to draw correlations between grains and conductivity. EDX shows which elements are where on a sample and what concentrations of those elements are present. This reveals how close to the targeted composition a sample is. While lithium is not picked up by EDX it still provides an additional analysis to compare to ICP-MS results.

2.2.3 Archimedes Density

Density is a necessary characterization for solid electrolytes in order to see porosity of a sample and analyze the microstructure. This helps to reveal correlations between density/porosity and conductivity for LLZO solid electrolytes. Relative density, experimental density divided by theoretical density, is the most accepted analysis as it gives reference to the targeted compositional density. The experimental density in this research was analyzed using Archimedes density. Archimedes density uses liquid displacement to accurately determine volume in the density equation,

$$\rho = \frac{m}{V}$$

where ρ is density, m is mass, and V is volume. Ethanol as used instead of water for LLZO so that the liquid would evaporate from the sample quicker. A sample is weighed dry and then saturated. The saturated weight is when the sample is suspended in the liquid and weighed while submerged. It is important to wait until the ethanol has seeped into the sample completely and there are no air bubbles seen on the sample while submerged. [46] This ensures the proper density and porosity are calculated. This method is more accurate than geometrical density because it factors in any air pockets within the

sample and air pockets are important to avoid when making solid electrolytes to ensure a conductive sample. The relative densities were calculated through the formula

$$\rho_{relative} = {}^{\rho_{experimental}}/_{\rho_{theoretical}}$$

where $\rho_{experimental}$ is measured by geometrical method and $\rho_{theoretical}$ is calculated using the lattice parameter and theoretical mass of the molecule.

$$\rho_{theoretical} = \frac{M \times ({}^{molecules}/_{unit\ cell})}{V \times N}$$

where M is the molecular weight of the composition, V is the volume of the unit cell, and N is Avogadro's number.

2.3 Electrochemical Impedance Spectroscopy (EIS) Testing

Electrochemical impedance spectroscopy (EIS) testing is the most vital data in solid electrolyte research. EIS analyzes the resistance and impedance of current flowing through the electrolyte between the two electrodes. [47] EIS works by sending an AC potential through an electrochemical cell and then measures the current that flows through. [48]

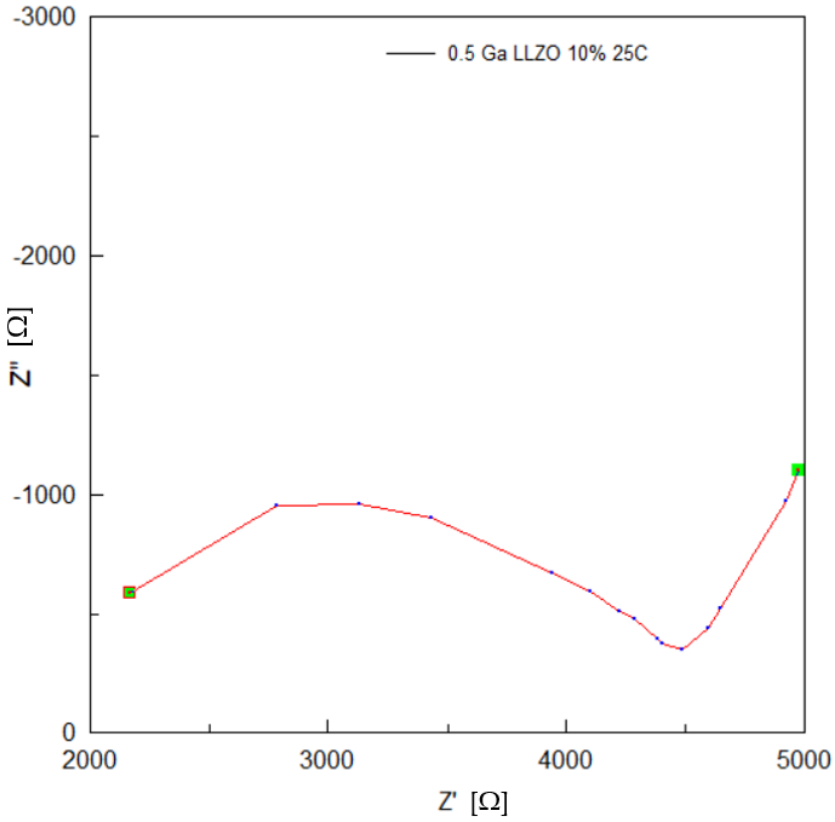

Figure 2-3 Impedance plot of Ga-LLZO electrolyte

EIS provides the impedance of the material in a graph form like in Figure 2-3. Using the shape of the hump before the 'tail' of the plot gives you the resistance. Resistance relates to voltage (V) and current (I) in Ohm's law:

$$R = V(t)/I(t)$$

Resistance is also related to conductivity (σ), length (L), and cross-sectional area (A).

$$R = \frac{1}{\sigma} \times \frac{L}{A} \quad \rightarrow \quad \sigma = \frac{1}{R} \times \frac{L}{A}$$

This equation will help to calculate the conductivity once we have the resistance. Once the EIS machine is turned on the AC signal is applied to the system. This excites and sends AC current through the pellet to measure the magnitude of current and phase . The sinusoidal voltage (V) of this process is shown as

$$V(t) = Vsin(\omega t)$$

where ω is the angular frequency.

Similarly, the sinusoidal current (I) is shown as

$$I(t) = Isin(\omega t + \phi)$$

where ϕ is the phase angle.

Resistance is also related to conductivity (σ), length (L), and cross-sectional area (A).

$$R = \frac{1}{\sigma} \times \frac{L}{A} \quad \rightarrow \quad \sigma = \frac{1}{R} \times \frac{L}{A}$$

The impedance of the sample, Z, can then be defined as

$$Z(t) = \frac{E(t)}{I(t)} = Z_0 \frac{\sin(\omega t)}{\sin(\omega t + \phi)}$$

The voltage can be extracted from this by using Euler's relation,

$$\exp(i\phi) = \cos(\phi) + i\sin(\phi)$$

and expressing impedance as a complex function,

$$E = E_0 \exp(i\omega t)$$

while current is described as

$$I(t) = I_0 \exp(i\omega t - i\phi)$$

Using these equations and expanding the Z component into its real and imaginary components reveals

$$|Z|^2 = (Z_{Real})^2 + \left(Z_{Imaginary}\right)^2$$

and a phase angle of

$$\tan(\phi) = \frac{Z_{Imaginary}}{Z_{Real}}$$

These equations and EIS testing allow researchers to analyze the Nyquist plots and reveal the conductivity of samples.

CHAPTER THREE

STRUCTURES

3.1 Tetragonal vs. Cubic Structures

Crystal systems play a crucial role in the characteristics of a solid-phase electrolyte. A crystal system describes the arrangement of atoms and what type of structure they form. LLZO is generally found in one of two structures, tetragonal or cubic. Cubic is the desired structure for solid state batteries due to its increase in conductivity compared to that of tetragonal (~10^{-4} S/cm and ~10^{-6} S/cm).

A tetragonal crystal system refers to a structure with three perpendicular axes, two of which are the same length. A cubic crystal system refers to a structure with identical lengths on all sides forming a cube shape. Figure 3-1 shows the a) tetragonal and b) cubic structures' shape for LLZO and the lattice parameters along with it. Both structures have a square base consisting of lattice parameter "a". The third lattice parameter, or height of the structure, is given by "a" for the cubic structure but for a tetragonal structure this third lattice parameter is a different number and labeled as "c".

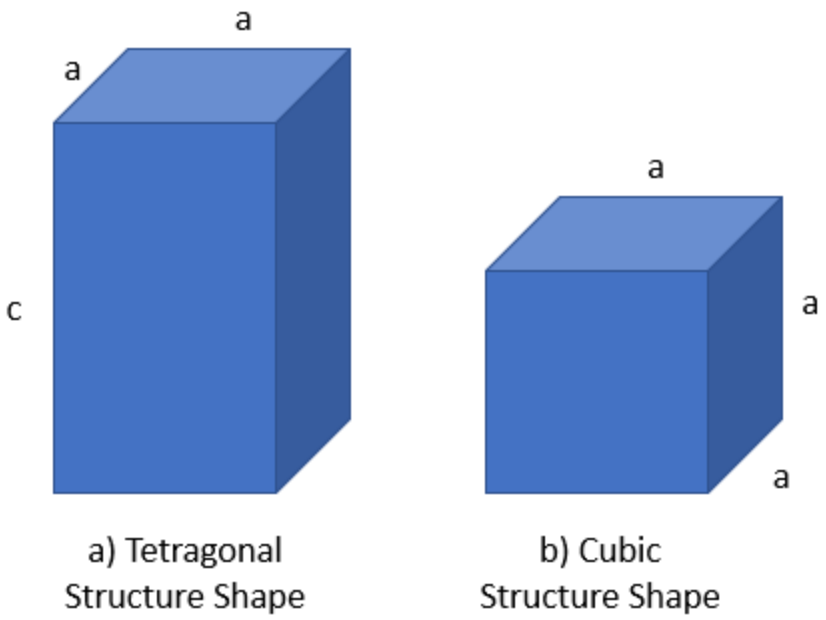

Figure 3-1 Lattice shapes and parameters for a) tetragonal and b) cubic structures

Figure 3-2 displays the XRD patterns of a tetragonal structure standard reference (ICSD *246816*) and a cubic structure standard reference (ICSD *182312)* of LLZO. [32], [49] These cubic and tetragonal standard reference phases correspond to the Inorganic Crystal Structure Database (ICSD) for tetragonal LLZO (*246816*) and cubic LLZO (*182312*). The tetragonal structure is part of space group Ia4d (ICSD_246816), while the stabilized cubic structure belongs to the Ia3d space group (ICSD_182312). [14] The tetragonal pattern in Figure 3-2 a) is evident in the (211) peak, magnified view which shows split peaks as compared to cubic structured materials. The (211) miller indice is critical for identifying the cubic LLZO structure, however it should be one peak rather than split peaks, (211) and (112). This split peak is showing the “a” and “c” lattice parameters indicating a tetragonal structure. The cubic pattern, Figure 3-2 b), shows one uniform peak at the (211) miller indice in the magnified view. This shows that cubic has

only ‘a’ as a lattice parameter which means that the volume is found from a^3 signifying a cubic structure, whereas the tetragonal contains ‘a’ and ‘c’ parameters with volume, a^2c.

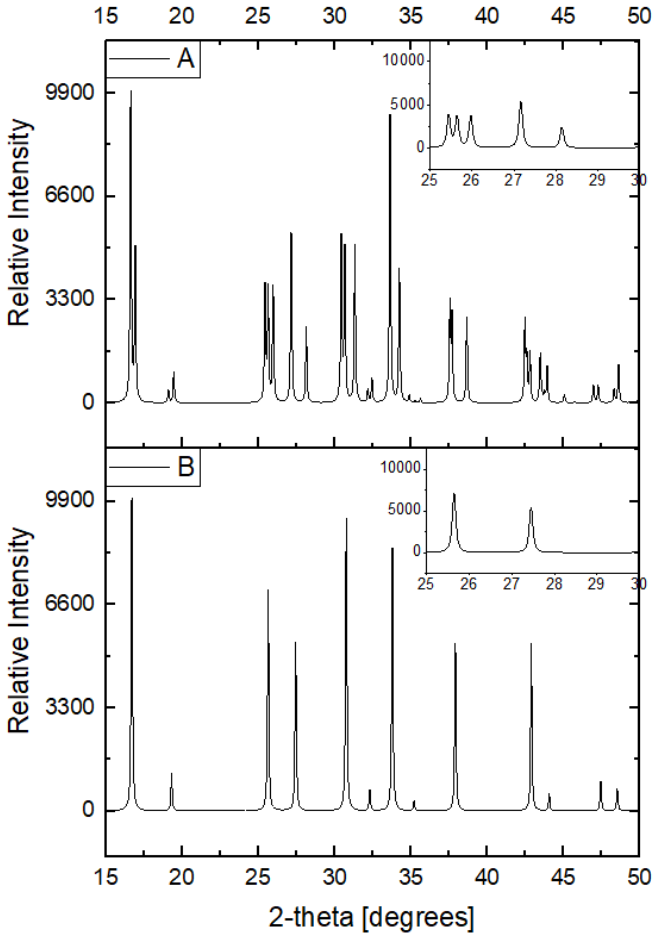

Figure 3-2 XRD patterns of a) tetragonal [50] and b) cubic reference phases [51]

Phase-pure cubic LLZO can only be made at room temperature through the quenching method. A cold pressed pellet of mixed precursors (Li_2CO_3, La_2O_3, and ZrO_2) is heated to the transition temperature to increase lithium ion pathways. There is a temperature dependency of lithium ion pathway formation. Thus, thermal motion ejects the lithium ions, which produces lithium ion vacancies. The pellet is then quenched to

maintain the cubic structure. This is a common method to maintain purity of the LLZO while also having a cubic crystal system.

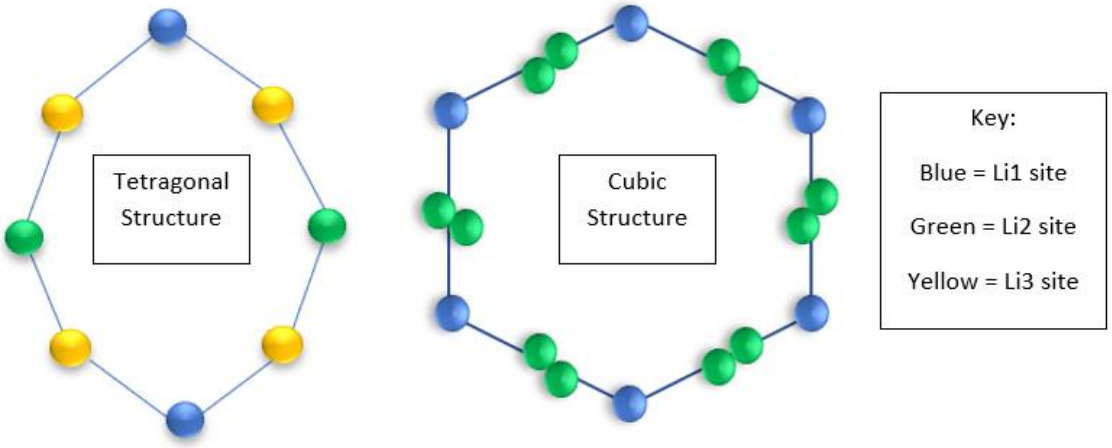

Figure 3-3 Illustration of lithium sites for a) tetragonal and b) cubic LLZO structures

Figure 3-3 displays a rendering to illustrate lithium site arrangements for tetragonal and cubic LLZO structures. The tetragonal structure has significantly fewer lithium sites than the cubic structure. The tetragonal structure is part of space group Ia4d (ICSD_246816), while the stabilized cubic structure belongs to the Ia3d space group (ICSD_182312). [14] The tetragonal arrangement depicts an oval shape with Li1 (8a), Li2 (16f) and Li3 (32g) sites. However, the cubic arrangement depicts a hexagonal shape with tetrahedral Li1 (24d) as well as octahedral distorted Li2 sites. [52] These shapes, and sites provide different characteristics to LLZO. For instance, the tetragonal LLZO tends to have fully occupied crystallographic lithium sites whereas cubic LLZO has reduced Li2 site occupancy and slightly lower occupancy of the Li1 site. [52] This increase in Li site vacancy in cubic LLZO corresponds to increased entropy. In the idealized cubic structure Li2 sites are vacant, however experimentally it is almost impossible to obtain

zero occupancy of Li2 sites. This disordering due to partial occupancy plays a major role in ion conduction for Li-ion conductors. [52] This disordering disrupts the long-range lithium order which leads to cubic structure and a high conductivity.

Lithium ion migration pathways should correspond to the lithium atomic arrangement in the structure. In Figure 3-3 the lithium diffusion pathways for tetragonal LLZO shows an oval structure with different lithium sites linked. The cubic structure shows a hexagonal structure with Li1 and Li2 sites. The tetragonal loop shows a further distance between the different lithium sites than in the cubic structure, while the cubic shows a more compact structure with consistent lithium sites around the edge. It is easier for lithium migration in cubic because of how close and how many lithium sites there are which is the reason cubic structure is necessary to attain. Naturally, pure LLZO at room temperature is always tetragonal. In order to achieve cubic structure, a dopant must be added, or a higher temperature must be sustained or quenched.

3.2 Dopants

Gallium dopant can be used to produce cubic LLZO by lowering the lithium content to produce Li vacancies disrupting the long-range lithium order. The means of phase transforming LLZO from tetragonal to stabilized cubic structure at room temperature without quenching requires a critical lithium vacancy concentration of 0.4 to 0.5 per LLZO formula unit, regardless of how these vacancies are introduced. [18] The dopant creates vacancies and stabilizes the cubic structure so that the LLZO will retain that cubic structure at room temperature. The dopant aids in increasing the degree of vacancy disorder within the lithium sublattice. [14]

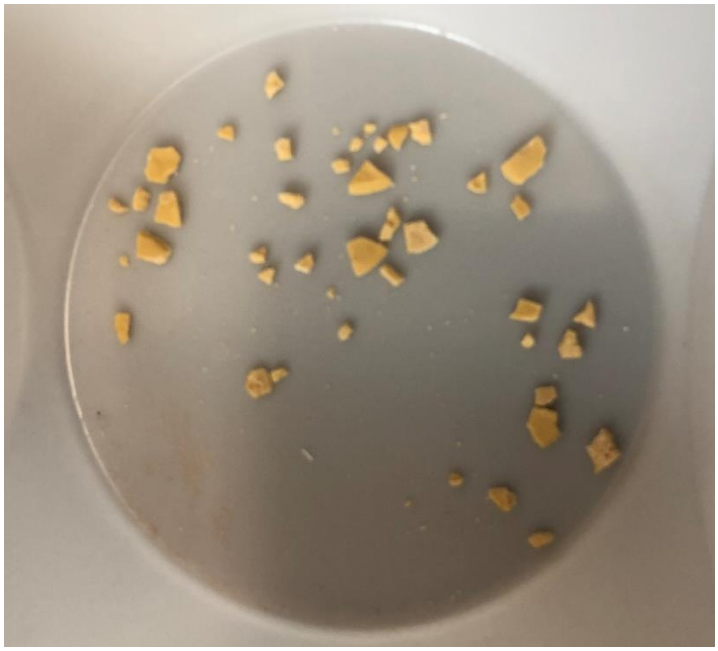

Figure 3-4 Photograph of melted aluminum doped LLZO pellets

In the initial stage of this project, aluminum and gallium dopants were attempted with LLZO to see which provide the best results. At the preliminary stages of this current project, aluminum samples were often melted to the crucible after sintering. A layer of doped mother powder was put below the samples prior to sintering but most samples still melted to the crucible and cracked as shown in Figure 3-4. This is likely due to a reaction between the alumina crucible and the aluminum doped LLZO sample. Liu et al reports a similar difficulty with alumina crucibles when the lithium salts decompose to Li_2O during sintering and reacts with Al_2O_3 in the crucible. [6] In order to prevent melting, other dopants were explored.

Gallium doped samples did not melt when mother powder was put below the pellets during sintering. The gallium dopant worked well and achieved cubic structure according to X-ray diffraction. 0.5 mol of gallium dopant was chosen based on

researching previous experimentation with gallium doped LLZO, 0.5 mol gallium always showed a cubic structure after sintering. [13], [20], [21] Ga_2O_3 (1,950℃) has a lower melting point that Al_2O_3 (2,072℃) which allows gallium doped LLZO to sinter at a lower temperature, 1,150℃, rather than the 1,220℃ necessary for aluminum doped LLZO. A lower sintering temperature is good because it promotes a better morphology. [13]

Wu et al prepared 0.1 Ga to 0.4 Ga doped LLZO samples for which 0.2 Ga or less produce below 90% density while samples with more than 0.2 Ga had densities of 93% and greater. [21] Their X-ray diffraction patterns also show 0.2 Ga and below have broadened peaks showing that they are not perfectly stabilized LLZO which could mean the presence of tetragonal structure. An increase in gallium content results in greater density, XRD, and EIS results.

Li et al (2017) investigated gallium doping to obtain cubic LLZO at 0.1 Ga, 0.5 Ga, and 1.0 Ga compositions. The X-ray diffraction patterns demonstrate that 0.1 Ga doped LLZO tetragonal structure with some presence of cubic. 0.5 Ga had cubic LLZO structure while 1.0 Ga doped LLZO had cubic structure with some presence of additional gallium resulting in a secondary phase formation. [21] A 0.5 Ga dopant was chosen to investigate in this research based on these results. 0.5 Ga LLZO shows cubic structure and no sign of secondary formations.

3.3 Excess Lithium

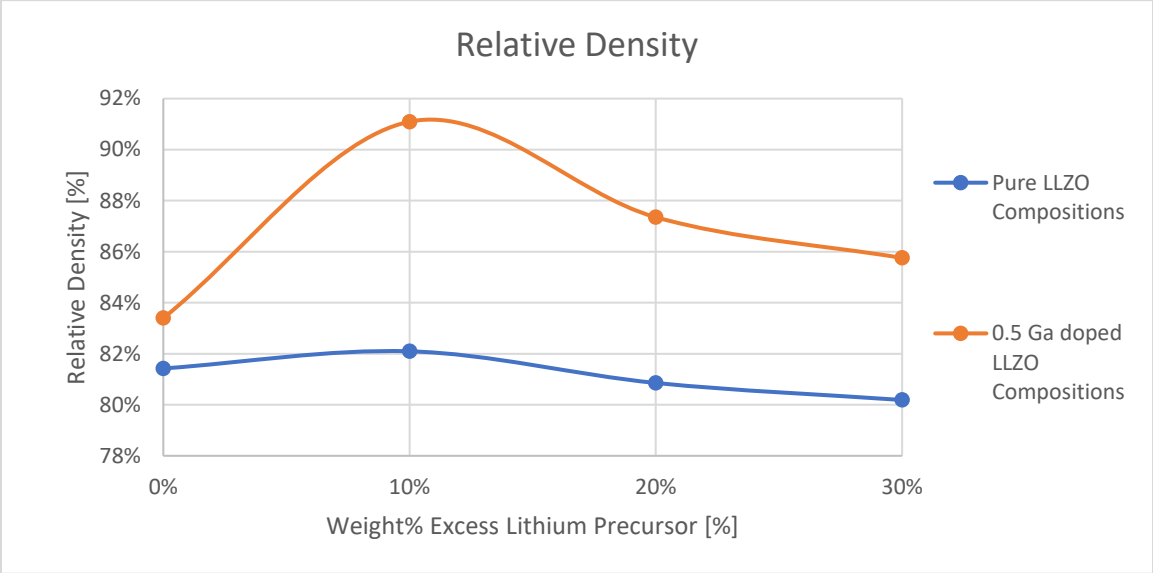

Figure 3-5 Plot of relative densities vs. weight percent excess Li

The change in density with respect to weight percent lithium concentration is presented in Figure 3-5. This figure shows the geometrical relative densities of Ga-LLZO samples and pure LLZO samples with various excess lithium precursor. This is the only time in this research where geometrical density is used, otherwise Archimedes method was used. The figure shows the increase in density between phase-pure LLZO tetragonal and Ga-doped LLZO cubic structures.

The orange line represents Ga-doped LLZO compositions. The pure LLZO compositions (blue line) are tetragonal and consistently have lower densities than their doped counterparts. The significant increase in density between Ga-doped and pure LLZO samples show the change in structure and the change in characteristics. While the densities all decrease after 10% excess for Ga-doped and pure LLZO samples, the Ga-doped line is always above the pure LLZO line. The XRD of the Ga-doped samples show

cubic structure while the XRD of the pure LLZO samples show tetragonal structure, this is supported by the increase in density with Ga-doped compared to pure LLZO.

The compact cubic structure allows lithium movement and provides the basis for a better solid electrolyte than a tetragonal and porous sample. The cubic structure is stable and more compact than the tetragonal structure. The cubic structure is the desired structure compared to tetragonal because cubic entails a denser material with increased lithium mobility which can lead to a higher conductivity. Cubic is also known to have a conductivity two orders of magnitude larger than tetragonal. While tetragonal is an easier structure to attain, it does not possess high conductivity that makes cubic LLZO ideal as a solid-state electrolyte.

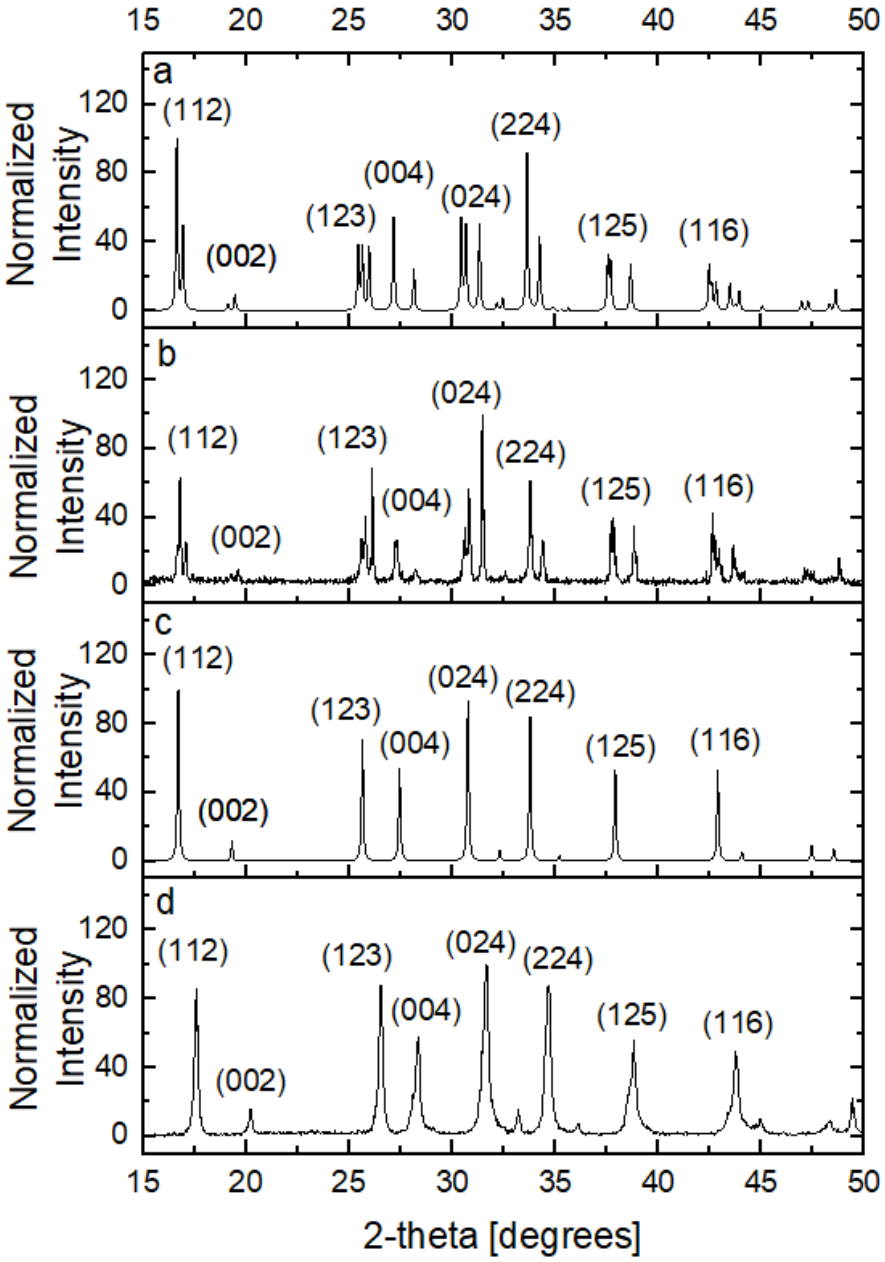

Figure 3-6 X-ray diffraction patterns of a) tetragonal LLZO reference [50] b) LLZO 10 c) cubic LLZO reference [51] d) Ga-LLZO 10

Figure 3-6 shows X-ray diffraction patterns. The two experimental compositions, Figure 3-6 b) and d), are the same except for the addition of a gallium dopant to one of them. Figure 3-6 d) displays uniform peaks corresponding to the cubic reference, Figure

3-6 c), while the experimental pure LLZO, Figure 3-6 b), presents split peaks corresponding the tetragonal reference, Figure 3-6 a). This shows the dopant is creating the proper lithium vacancy concentration so that there are increased lithium ion migration pathways to attain a cubic crystal system.

Cubic LLZO can be seen on XRD by presenting peaks at certain miller indices to indicate a cubic structure. Cubic LLZO has critical peaks at (112), (022), (123), (004), (024), (224), (125), (116), and (246) all ranging between ten to sixty 2θ. [26] These peaks will be uniform, single peaks at each miller indice if the sample is phase-pure cubic. However, if the peaks at these miller indices show splits that shows that there is some tetragonal formation and the sample is not fully stable cubic.

The reference cubic pattern shows clean lines which indicates a fully stable cubic structure. The doped LLZO samples show similar clean lines as the cubic reference pattern. However, pure LLZO samples all show 'noisy' lines on their XRD pattern showing the instability and tetragonal structure. This 'noise' also shows split peaks where the reference shows a single, uniform peak. The split peaks show tetragonal instability and different products besides LLZO. It is imperative to see clean peaks for LLZO to ensure cubic structure is attained. Cubic structure is the only structure of LLZO with beneficial characteristics for conductivity.

Figure 3-6 shows very similar XRD patterns for the pure $Li_7La_3Zr_2O_{12}$ and the reference tetragonal pattern. Both show 'split-end' peaks, where the peak that corresponds with the cubic reference is instead split into two separate peaks not quite on the same degree as the cubic single peak is. This shows the tetragonal structure rather

than the cubic because the peaks are split and not uniform single peaks as shown in the cubic reference.

Figure 3-6 a) and b) shows very similar ‘split-end’ peaks for the pure $Li_7La_3Zr_2O_{12}$ and the reference tetragonal pattern. The cubic reference pattern and the $Ga_{0.5}Li_{5.5}La_3Zr_2O_{12}$ sample also look very similar with uniform, single peaks. The Ga-doped sample pattern and the cubic pattern have no split peaks at any point show, which exemplifies the stabilized cubic structure.

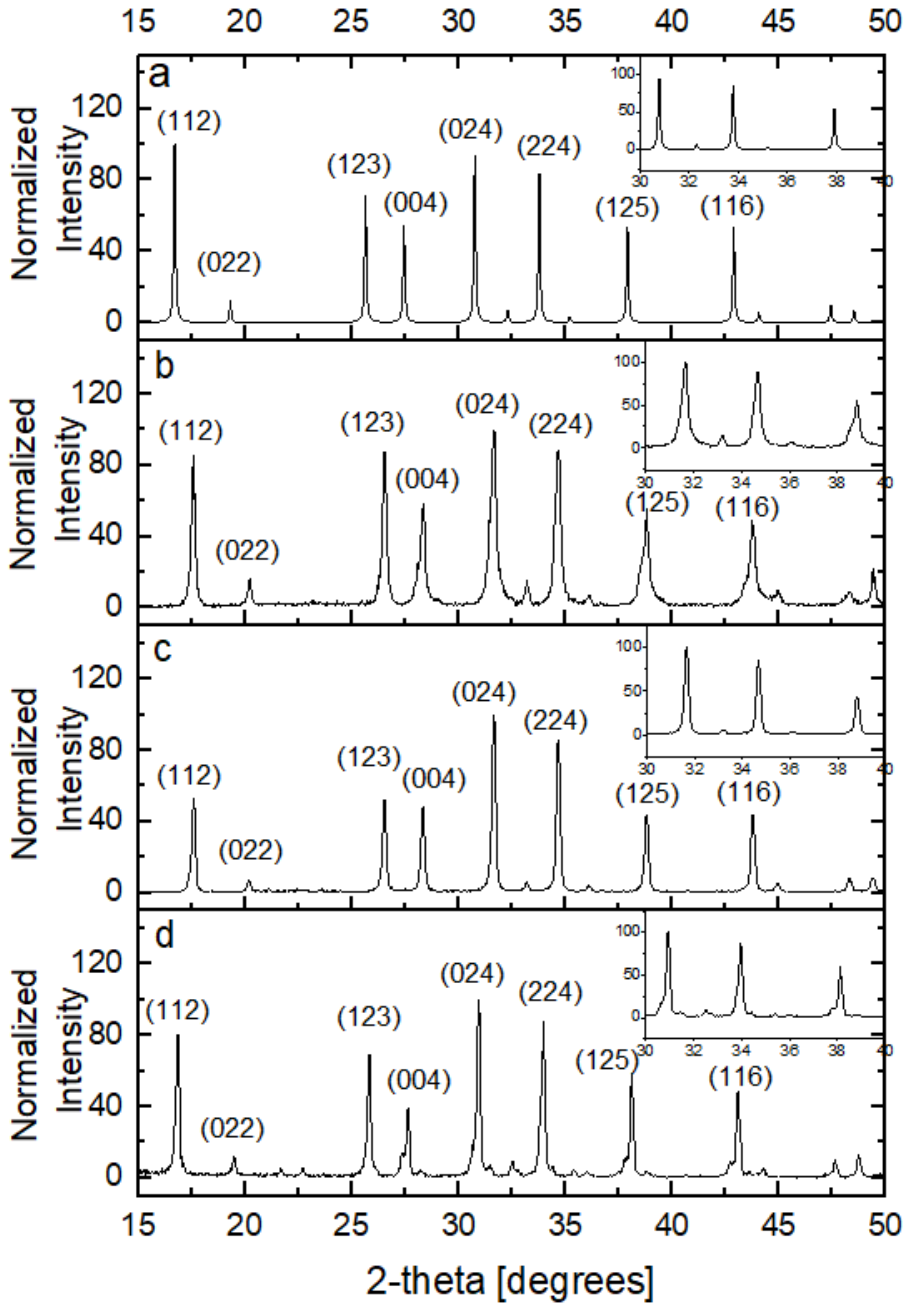

Figure 3-7 XRD patterns for a) cubic LLZO reference [51] b) Ga-LLZO 10 c) Ga-LLZO 20 d) Ga-LLZO 30

Figure 3-7 shows the X-ray pattern of $Ga_{0.5}Li_{5.5}La_3Zr_2O_{12}$ with ten, twenty, or thirty weight percent excess lithium precursor. The top pattern shows the cubic reference

of how a proper cubic LLZO pattern should look. As the amount of excess lithium precursor increases, the peaks line up better with the reference XRD pattern. Ga-LLZO with thirty percent excess lithium precursor shows pattern peaks that line up almost exactly to the cubic reference lines. This shows that the excess lithium precursor helps to stabilize the structure and attain a cubic form.

The excess lithium is added in order to compensate for the lithium loss during sintering so that cubic structure can be attained. If there is too much lithium loss then the pyrochlore phase is often made, $La_2Zr_2O_7$. This phase has a low conductivity so excess lithium is usually added to LLZO to avoid the pyrochlore phase. The difficulty is figuring out the proper amount of excess lithium to add in order to avoid the pyrochlore phase and achieve a phase-pure stable cubic structure. Figure 3-7 displays the experimental XRD patterns getting more in line with the cubic reference as more lithium is added. This could mean that more than the standard 10 weight percent excess is necessary to for phase pure cubic LLZO.

The middle two patterns show similar peaks with different intensities, however they both show peaks slightly to the right of the cubic reference. This likely indicates a change in lattice parameters. As the diffraction peaks shift, the lattice parameter is changing from the targeted lattice parameters that the cubic reference possesses. The shift to the right indicates the lattice parameters are smaller than the reference. This is likely due to the lack of lithium in the composition due to lithium evaporation during sintering. This is further shown with the last pattern, 30% excess lithium precursor, where its peaks almost exactly match up with the cubic reference.

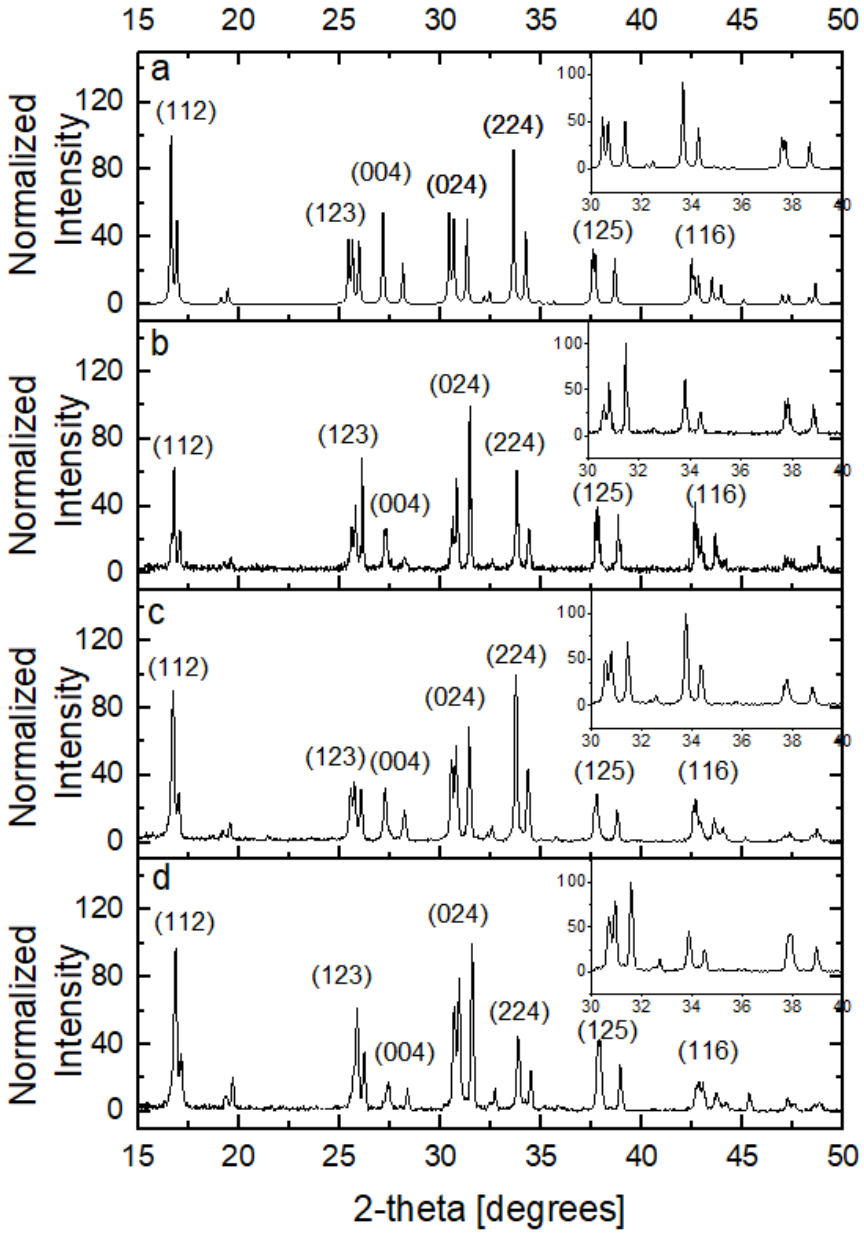

Figure 3-8 X-Ray patterns for a) tetragonal LLZO reference [50] b) LLZO 10 c) LLZO 20 d) LLZO 30

Figure 3-8 shows XRD patterns of every pure LLZO composition with excess lithium precursor. The top pattern exemplifies the tetragonal LLZO XRD pattern as a

reference to how close each composition got to perfect compositional structure. The figure shows that the pure composition with ten percent excess lithium precursor show peaks slightly to the left of the reference lines. This shows the struggle of the composition to try to reach cubic, but it does not have the proper stabilization to reach there.

While the pure compositions will not show cubic structures due to the lack of a dopant and no quenching during synthesis. The pure compositions are all tetragonal, however it is important to note that as the excess lithium precursor amount increased with the pure compositions. The tetragonal reference lines match up more precisely with the alpha lattice parameter peaks. This shows the excess lithium helps to make up for lithium loss in order to still have the proper composition wanted.

While the pure compositions line up better with the tetragonal reference than the doped compositions did, the intensity of the pure LLZO patterns steadily increases as the excess lithium precursor increases. The excess lithium precursor is necessary to account for lithium loss and attain the proper composition with a strong intensity. The compositions with less excess lithium precursor struggle with this compared to those with more excess lithium precursor.

Sample Name	a (angstroms)	c (angstroms)	Phases Present
LLZO with 10% excess Li	12.399	10.647	Tetragonal
LLZO with 20% excess Li	12.409	10.676	Tetragonal
LLZO with 30% excess Li	12.378	10.611	Tetragonal
0.5 Ga LLZO 10% excess Li	12.929	N/A	Cubic
0.5 Ga LLZO 20% excess Li	12.950	N/A	Cubic
0.5 Ga LLZO 30% excess Li	12.899	N/A	cubic

Table 3-1 Lattice parameters of different compositions

The cubic lattice parameter, a, illustrated in Figure 3-1 b) are calculated by the d-spacing and h k l coordinates at various peaks. The d-spacing and h k l coordinates are found using Jade 5 software. Those values are then inserted into the following equation

$$\frac{1}{d^2} = \frac{h^2 + k^2 + l^2}{a^2}$$

While the tetragonal lattice parameters, a and c, illustrated in Figure 3-1 a) are found by using the d-spacing and h k l coordinates in the following equation

$$\frac{1}{d^2} = \frac{h^2 + k^2}{a^2} + \frac{l^2}{c^2}$$

Table 3-1 shows the lattice parameters and structures present for each composition. It is important to note that it does not matter if the samples have exterior excess lithium addition in this testing as the XRD testing was done on the powders before they are cold pressed to pellets and sintered for this data collected. The table shows similar numbers for doped compositions and similar for pure compositions. The trend shows that the twenty percent excess lithium precursor compositions for both pure and doped samples have the largest lattice parameters. Both doped and pure show an increase in lattice parameters between the ten percent and twenty percent excess lithium precursor. However, in both pure and doped compositions the lattice parameters decrease by a little from the twenty percent to thirty percent excess lithium precursor. Large grains are preferable as it shows the grains grew during firing and hopefully grew uniformly so the material will be denser. It is expected that as more excess lithium is added, the grains will be larger since it should be closer to the targeted composition, however the data shows a decrease for the thirty weight percent excess samples signifying there is an ideal amount of excess lithium to add.

The proper amount of excess lithium is important in LLZO to ensure a cubic crystal system. If too much lithium is lost during sintering, then there will be too many lithium vacancies and if there is too much lithium then there will be too few vacancies for a cubic structure. This can be shown as the thirty percent excess lithium had smaller lattice parameters than samples with less excess lithium, though all lattice parameters were similar sizes.

CHAPTER FOUR

MICROSTRUCTURES

4.1 Background on Microstructures

While crystal structure describes the arrangement of atoms in a material, the microstructure describes a single crystal or polycrystal. The crystals microstructure or morphology is described through phases present, grain boundaries, grain size, cation ratios, and more. [53] Characterizing the microstructure presents the physical properties of the material from a microscopic level which allows researchers to predict the behaviors of the entire material. Microstructure is important to research with solid state electrolytes because for many applications it is necessary that the electrolyte has high Li-ion conductivity, low electronic conductivity, chemical stability with anodes, and adequate mechanical properties. [11] If a solid-state electrolyte can exhibit all these properties, then the electrolyte proves to be a viable long-term option.

The microstructure can be altered by many different factors such as crystal structure, size, shape and orientation, or the chemical composition of the grains. [54] While most materials characterization depends on the precursors and sintering temperature, the microstructure can be changed from precursors or sintering and every step in between. The processing procedures when making a sample is integral to the materials morphology. If two samples with the exact same precursors and sintering temperature are prepared in two different ways, the microstructure will show these differences and how the preparation methods compare. In one study, the Al-substituted

cubic garnet like LLZO dispersed in a poly (ethylene oxide) matrix as their solid electrolyte preparation. The study reveals that this preparation method leads to a reduction in electrochemically inactive components boosting the conductivity of the sample. [55] The preparation method in this study changed the microstructure of the sample leading to a higher conductivity than without using the method.

Microstructure examination is performed using a scanning electron microscope (SEM), as described in chapter two, in order to magnify the features of each grain on the materials surface. LLZO oxidizes easily when exposed to air and can show only the oxidized layer in the SEM. In order to combat this the cross section of each sample was used to characterize the microstructure so that an accurate representation of the material is shown.

4.2 Excess Lithium Processes

LLZO has high conductivity in its cubic structure making it an ideal candidate for a solid electrolyte, however sintering LLZO to become cubic can lead to some lithium loss. Lithium melts at 180.5℃ and Li_2CO_3 melts at 723℃ which are much lower than the calcine and sinter temperatures of 1050℃ and 1150℃ respectively. [56] This discrepancy in temperature can lead to lithium loss altering the LLZO product. If too much lithium evaporates it can result in the pyrochlore phase, $La_2Zr_2O_7$, which has a low conductivity. [57] In order to avoid this pyrochlore phase it is imperative to maintain as much lithium as possible. Besides achieving the wrong composition, lithium content is important to maintain high density and high conductivity.

In order to maintain lithium content in the LLZO product there have been various strategies on how to go about it. The most researched and documented method is to add excess lithium precursor. [12], [19] This method allows for there to be excess lithium present when some lithium evaporates. When some of the lithium evaporates and creates too many vacancies, there will be excess lithium to fill some of those vacancies. The difficulty with this method is figuring out what amount of excess lithium precursor will result in the highest conductivity and highest density.

In a study, zero to fifty mol percent excess lithium increasing by ten percent was tested. [12] Their sample is similar to this research but with a different dopant, tantalum rather than gallium. While the different dopants may be hard to compare, the excess lithium with a controlled dopant is the same set up so the change between different excess lithium amounts is comparable. The results show increased conductivity until 40 mol% excess lithium where the conductivity is 3.72×10^{-4} S/cm while the 30 mol% excess lithium boasts a conductivity of 4.33×10^{-4} S/cm. [6] This discrepancy suggests that beyond 30 mol% excess lithium the benefits of the excess lithium are outweighed by its cons. This is supported further as the 50 mol% excess lithium has a conductivity of 3.66×10^{-4} S/cm, which is lower than the 40 mol% conductivity. This bell curve shape of conductivity as excess mol% lithium increases suggests that somewhere around 30 mol% excess lithium is the ideal ratio needed to maximize conductivity.

In order to test the ideal amount of excess lithium to add, this research tests ten to thirty weight percent excess lithium as well as no excess as a control as displayed in

Table 4-1. These different excess amounts should help to clarify the ideal amount of excess lithium to add to pure LLZO or gallium doped LLZO.

The amount of excess lithium precursor to add into the $Li_7La_3Zr_2O_{12}$ is done using the stoichiometrically calculated grams for the lithium in $Li_7La_3Zr_2O_{12}$ and multiplying the grams by 1.1 for 10% excess, 1.2 for 20% excess, and 1.3 for 30% excess. The number calculated is the total number of grams of Li_2CO3 to add to the other precursors. This excess lithium precursor is added to the sealed mixing container and ball-milled along with the other precursors for at least 24 hours as detailed in the experimental methods chapter.

Base Powder	Excess Lithium Precursor Amounts (weight%)
$Li_7La_3Zr_2O_{12}$	0%, 10%, 20%, 30%
$Ga_{0.5}Li_{5.5}La_3Zr_2O_{12}$	0%, 10%, 20%, 30%

Table 4-1 Excess lithium precursor compositions

The pure and doped LLZO both had control compositions with no excess lithium precursor or additive as well as samples with ten, twenty, and thirty percent excess weight percent lithium precursor. These samples were tested as well as another set of the same compositions, but they also used the boating technique creating twice as many unique samples.

4.3 Microstructure Results

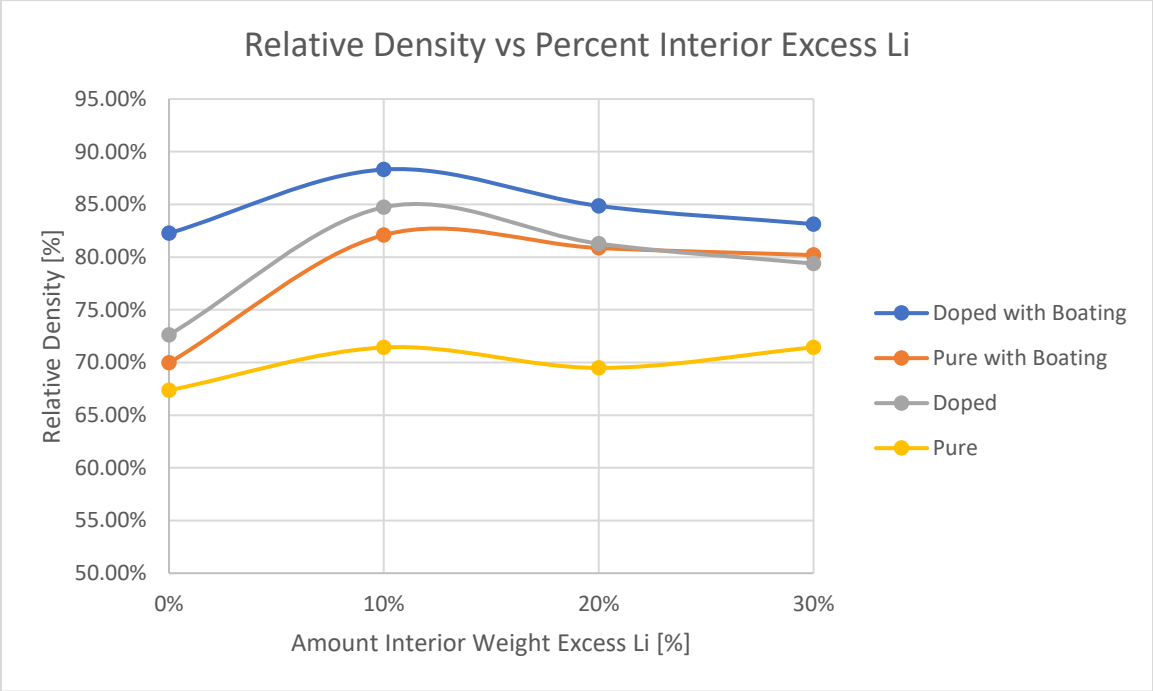

Figure 4-1 Plot of relative density vs. interior excess lithium

Figure 4-1 shows the change in Archimedes relative density as the excess lithium increases in weight percent. The relative density is calculated similarly to Figure 3-5 however Figure 4-1 displays the Archimedes density for the actual density. The different compositions and preparation methods used in this research can be broken down into the four categories of ‘pure’ LLZO, ‘doped’ LLZO, ‘pure with boating’ LLZO, and ‘doped with boating’ LLZO. Every composition was prepared with no excess lithium precursor as well as ten, twenty, and thirty percent excess lithium precursor.

The only composition and preparation method that had consistent relative density results above eighty percent were the compositions utilizing the gallium dopant as well as the boating preparation technique, described in the experimental methods chapter. In the

structures chapter, it was discussed how the dopant aids in a higher density for LLZO compositions compared to pure-phase LLZO without a dopant. Now, the results also add in the boating technique to see how that excess lithium gas pressure can aid in achieving higher density. The doped samples have the second highest relative densities, but the doped samples with the boating technique remain denser than without using the boating technique. Utilizing the boating technique allows extra pressure in the crucible during sintering to build up to press on the pellet creating a denser pellet than without excess pressure during sintering.

At zero excess lithium, both doped and pure LLZO show low densities of 65-75%. The pure and doped compositions with boating show 70-85% relative density at zero excess lithium. The boating technique consistently shows higher density than their non-boating counterparts. At 10 wt% the density of each composition increases showing that the excess lithium precursor aids in densifying the sample. The 20 wt% excess compositions of every sample type show slightly lower densities than their 10% counterparts suggesting that around 10 wt% excess lithium is ideal.

Composition Shorthand	Targeted	EDX	ICP-MS
LLZO 10	$Li_7La_3Zr_2O_{12}$	$Li_XLa_3Zr_{1.787}O_{12}$	$Li_{7.297}La_3Zr_{2.02}O_{12}$
Ga-LLZO 10	$Ga_{0.5}Li_{5.5}La_3Zr_2O_{12}$	$Ga_{0.475}Li_XLa_3Zr_{1.486}O_{12}$	$Ga_{0.482}Li_{5.981}La_3Zr_{2.13}O_{12}$

Table 4-2 Targeted compositions vs. experimental compositions

Table 4-2 displays the molecular formulas of two compositions based on the measurements from EDX and ICPMS. The ICPMS shows more accurate results and is sensitive enough to pick up the lithium content whereas EDX is not able to. The lanthanum content is held at its targeted amount to help calculate the other elements. The pure LLZO with ten percent excess Li shows a targeted composition of $Li_7La_3Zr_2O_{12}$ which is the general formula for LLZO. The experimental ICPMS data shows the pure LLZO with ten percent excess shows a similar composition as the targeted, the lithium and zirconium contents are slightly higher than targeted. While the EDX data of the pure LLZO composition shows less zirconium than the targeted composition. This discrepancy shows how EDX is not as accurate as the ICPMS. The ICPMS picks up on virtually every amount of every element while EDX does a scan over the surface of a sample. The important thing to notice is how close the EDX and ICPMS data are to the targeted. While there is a discrepancy between them, the targeted composition is between both experimental data revealing that both the EDX and ICPMS give proper results with ICPMS being more accurate and closer to the targeted.

In Table 4-2 the Ga-LLZO with ten percent excess Li precursor shows the targeted composition of $Ga_{0.5}Li_{5.5}La_3Zr_2O_{12}$. The EDX and ICPMS data in this case provide very similar results for the gallium content. The targeted gallium content is 0.5, while the EDX and ICPMS present 0.475 and 0.482 respectively. For the other elements, Li and Zr, ICPMS shows more than the targeted amount while EDX shows less Zr than the targeted amount. In the doped composition the zirconium content shows the most deviation between the different methods. EDX reveals 1.486 while ICPMS contains 2.13.

This shows that not all the elements are consistent between the two methods, gallium was very similar while zirconium content has more deviation. The contents of each sample can be altered through preparation methods as well as what method is used to calculate elemental content.

Sample	Targeted La:Zr ratio	EDX La:Zr ratio	ICP-MS La:Zr ratio
LLZO 10	3:2	3:1.786	3:2.020
LLZO 20	3:2	3:1.686	
LLZO 30	3:2	3:1.594	
Ga-LLZO 10	3:2	3:1.386	3:2.126
Ga-LLZO 20	3:2	3:1.473	
Ga-LLZO 30	3:2	3:1.467	

Table 4-3 Experimental compositional cation ratios

While compositional analysis reveals the total molecular formula, it is important to investigate the cation ratio behavior as well when investigating microstructure. The cation ratio impacts the composition of the sample and will affect the microstructure of the sintered product. In a separate study the cation ratio is shown to help influence the nature of crystallization for the product, however it did not affect the grain size. [58] The cation ratio can impact the sample in certain way but will not necessarily affect every aspect of structure or microstructure.

Table 4-3 presents the cation ratios calculated from EDX and ICPMS. Only two samples were sent to ICPMS and therefore only show ratios for the samples tested. Pure

LLZO shows the cation ratio grows as more excess lithium precursor is added. As more excess lithium is added to the LLZO precursors it results in less zirconium content. While the ICPMS data shows the smallest ratio for pure LLZO for the pure LLZO with ten percent excess lithium sample. However, the Ga-LLZO data shows no trend, the ratio gets smaller between ten and twenty percent excess lithium precursor for Ga-LLZO. The Ga-LLZO with thirty percent excess lithium precursor reveals a similar ratio as the twenty percent excess Li Ga-LLZO. The ICPMS data shows that zirconium content is much higher than the EDX data reveals in Ga-LLZO data, which means there is likely a discrepancy in the EDX data as it is not as accurate as the ICPMS data. The lack of trend for the Ga-LLZO suggests that the cation ratio does not play as much of a role in the microstructure for doped LLZO.

Sintering LLZO is meant to grow the grains larger to densify the material and allow for more conductive bulk ion transport pathways. In Figure 4-2 the SEM cross-sectional images of the different pure LLZO compositions at 1000 times magnified. In Figure 4-2 a) the pure LLZO with no additives is shown with visually smaller grains than the compositions with excess lithium precursor. This reveals that the excess lithium precursor helps attain larger grains during sintering. It is more difficult to visually see a difference between the compositions with excess lithium precursor as they all have similarly large grains, calculated grain size is shown further down to compare these sizes. Figure 4-2 b) LLZO with ten percent excess lithium precursor shows smaller grains than d) LLZO with thirty percent excess lithium precursor. This further exemplifies the importance of excess lithium precursor with grain size.

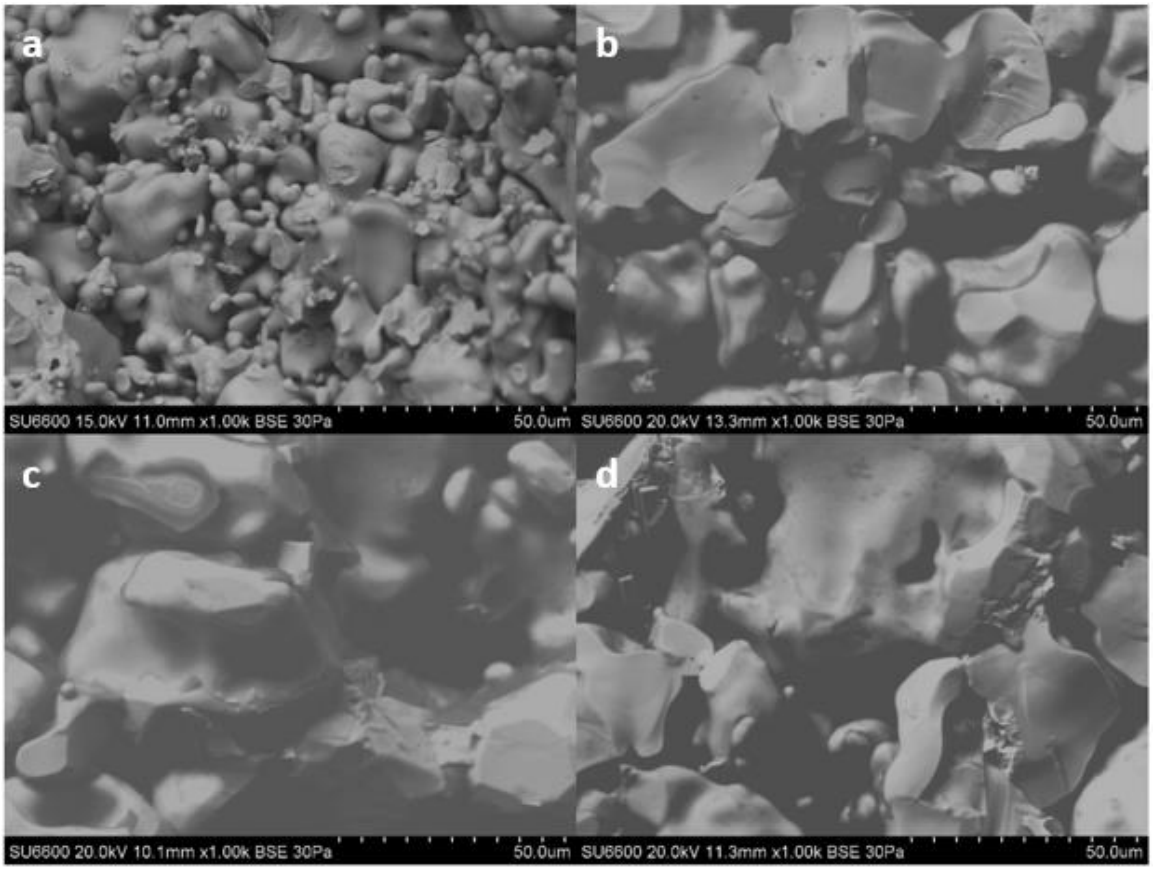

Figure 4-2 SEM images of a) pure LLZO b) LLZO 10 c) LLZO 20 d) LLZO 30 at 1000X

It is important to also consider grain shape when looking at SEM images of samples. The grain shape should be uniform throughout the sample in an ideal situation. In Figure 4-2 every image shows variously sized grains. This shows that there is not as much uniformity as there should be to produce a dense and conductive sample.

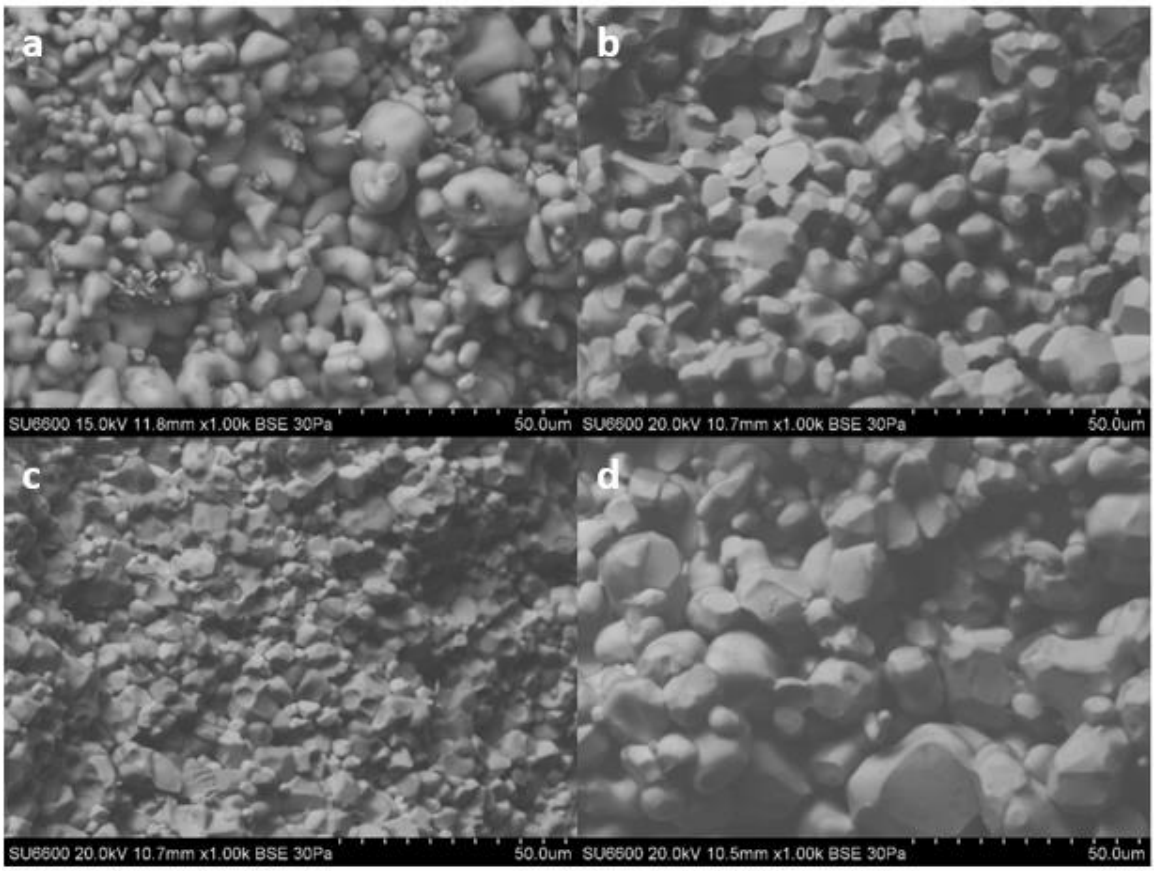

Figure 4-3 SEM images of a) Ga-LLZO b) Ga-LLZO 10 c) Ga-LLZO 20 d) Ga-LLZO 30 at 1000X

Figure 4-3 presents the SEM images of Ga-LLZO compositions at 1000 times magnification to investigate grain size and shape. It is more difficult to see a visual change between these images compared to Figure 4-2 which showed more extreme differences in grain size. However, the uniformity in grains in Figure 4-3 is evident. In Figure 4-3 a) the grains seem to have many different shapes and sizes but as there is more excess lithium precursor added, the grains become more uniform looking as seen in Figure 4-3 d). Figure 4-3 a) does show visually smaller grains than 4-3 d), while it is not as abrupt a change as Figure 4-2, it is still evident that the grains grow larger with more

excess lithium precursor added. The grain sizes and standard deviations can be seen below in Table 4-4 to present the grain sizes in a more quantifiable manner.

Sample Composition	Mean Grain Size [μm]	Standard Deviation	N (# of grains)
Pure LLZO	1.032	0.521	60
LLZO 10% Li	1.523	0.701	50
LLZO 20% Li	2.110	0.883	55
LLZO 30% Li	2.107	0.816	45

Table 4-4 Mean grain size of pure LLZO samples

Table 4-4 lists the different pure LLZO compositions and their corresponding average grain size and standard deviation which correspond to the SEM images in Figure 4-2. The grain size increases as more excess lithium precursor is added except for pure LLZO with thirty percent excess lithium, which is about the same as the twenty percent excess Li composition. This increase in grain size shows that the excess lithium precursor aids in increasing grain growth during sintering. It is also important to note that as the average grain size grew the standard deviation between grain sizes also grew meaning there is less uniformity in the grains as the grain sizes get larger. The ideal sample has large grains and uniform grains meaning a high average grain size and low standard deviation is preferred.

Sample Composition	Mean Grain Size [μm]	Standard Deviation	N (# of grains)
0.5 Ga LLZO	0.987	0.485	65
0.5 Ga LLZO 10% Li	1.450	0.319	57
0.5 Ga LLZO 20% Li	1.152	0.334	63
0.5 Ga LLZO 30% Li	1.864	0.590	50

Table 4-5 Average grain size of gallium doped LLZO samples

Table 4-5 displays the average grain sizes of the Ga-LLZO samples with various amounts of excess lithium precursor. These grain sizes correspond to the SEM images in Figure 4-3 for reference. 0.5 Ga-LLZO with no excess lithium shows the smallest average size with the largest standard deviation. This reveals that the additives help to increase grain size and lower standard deviation. When ten percent excess lithium precursor is added, the average grain size grows by 0.463 or a 47% increase in average grain size. This growth in grain size is important for a beneficial microstructure, but it is also important to notice that the standard deviation in grain size went down 34% between the Ga-LLZO with no additives to the Ga-LLZO with ten percent excess lithium precursor. This data suggests that as the excess lithium precursor is added, the grains grow and become more uniform.

There are exceptions to the general trend of data like the 0.5 Ga-LLZO with twenty percent excess lithium precursor. The grain size went down between ten and twenty percent excess lithium which does not correspond to the pure LLZO data shown

in Table 4-4. This can be caused from the preparation methods, for example if the crucible was not properly sealed, this sample could have sintered improperly leading to less than ideal grain size and shape. There is, however, a significant increase between the thirty percent excess and the ten and twenty percent Li excesses. The Ga-LLZO thirty percent excess Li composition shows the largest average grain size for the Ga-LLZO compositions; however, it also shows the largest standard deviation meaning while the grains are overall larger, they are not as uniform as other samples.

The standard deviation in the pure LLZO samples were all above 0.52 while the largest standard deviation for the Ga-LLZO is 0.590. This drastic difference in standard deviations suggests that the gallium dopant promotes a uniform growth in grains during sintering rather than its non-doped counterparts.

The microstructure of a sample describes the behavior and structure of a crystal within a sample. This information allows researchers to analyze how a sample will behave in different applications by knowing how each crystal behaves. The microstructure in LLZO is important in order to determine that there will be highly conductive results. The actual composition of LLZO plays a role in this as lithium content is a large concern in this area of research. The ICPMS data proved that the actual compositions are like the targeted and the EDX data helped to back this up.

The microstructure also depends on the grain size, grain shape, and density of the material, all of which play into providing a conductive material. The densest composition found was the 0.5 Ga-LLZO with ten percent excess lithium precursor as well as the boating technique. This superior density compared to other compositions and preparation

methods shows that the interior excess lithium precursor and the boating technique are both necessary to produce to a dense LLZO sample. The grain sizes and grain shapes in tables 4.4 and 4.5 reveal that while pure phase LLZO with twenty percent excess lithium precursor has the largest grain size of 2.110 μm it also has the highest standard deviation of 0.883. The large standard deviation detracts from the large grain size because this means the uniformity is lacking. The overall best grain size is 0.5 Ga-LLZO with thirty percent excess lithium precursor due to its large grain size of 1.864 μm and a lower standard deviation of 0.590. This is the best overall sample as it has the best trade-off between uniform grains and large grains.

CHAPTER FIVE

ELECTROCHEMICAL RESULTS

5.1 Conductivity Testing Background

Solid-state batteries must enable solid state ionic transport of a similar magnitude that is found with ionic transport in organic liquids used in conventional batteries in order to be a viable substitute. [10] Ionic conductivity occurs when the movement of charged ions jump from lattice site to lattice site under the influence of an electric field. The driving force for this electric field are the reactions that occur at the cathode. [59] Ionic conductivity depends on the lithium ion migration, crystal structure, and grain structure. The crystal system and microstructure influence how conductive a material will be.

The ionic conductivity of the LLZO samples were investigated using AC impedance electrochemical spectroscopy (EIS) using silver electrodes on either side of each sample. Silver paste is heated at 700℃ for an hour in order to remove any organic material in the silver paste. The sample's conductivity is then tested from 50 to 450℃ to see how temperature influences conductivity as well.

EIS testing provides a nyquist plot, like the one displayed in Figure 5-1, with the conductivity results. A nyquist plot plots the real Z component on the X-axis and the imaginary Z component on th Y-axis. The plot shows a semicircle and a tail, revealing high and low frequencies respectively. Based on this plot the resistance can be found, made up of bulk, grain-boundary, and electrode resistances. The impedance is then calculated by $(R_{bulk})(R_{grain\text{-}boundary}Q_{grain\text{-}boundary})(Q_{electrode})$, where R is the resistance and Q is the constant phase element contribution. [32] The nyquist plot reveals the Z values, real

and imaginary components, to be able to then calculate the resistance and conductivity to be able to create an arrhenius plot.

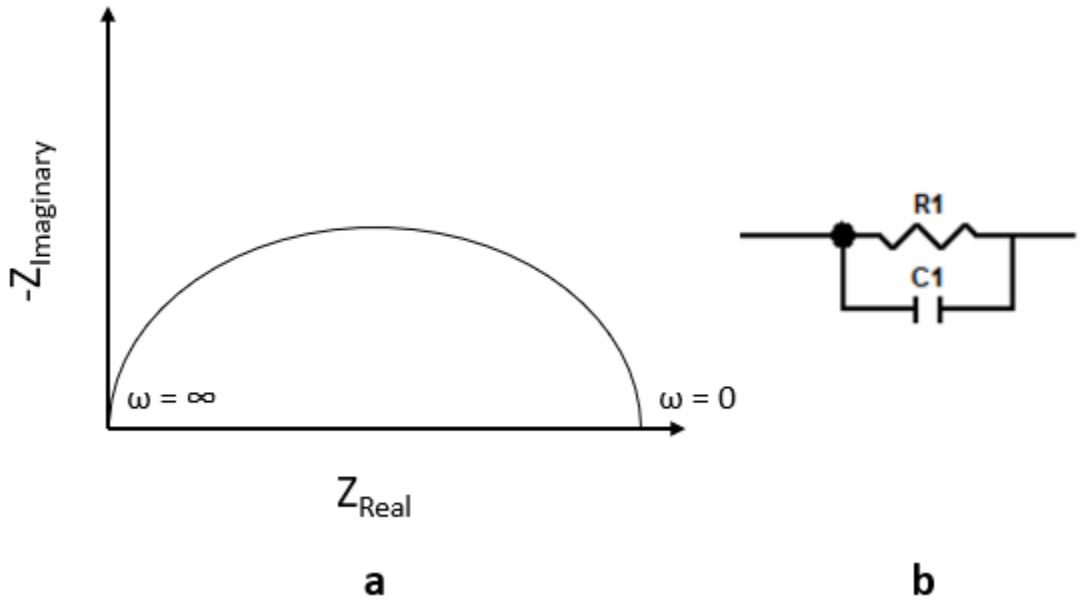

Figure 5-1 Illustrations of a) nyquist plot of RC pattern and b) circuit equivalent of RC pattern

The Z value and its components can be denoted as,

$$Z(\omega) = Z_{Real} - \acute{\imath}Z_{Imaginary}$$

The Z components can calculate the magnitude of Z through the equation,

$$|Z|^2 = (Z_{Real})^2 + (Z_{Imaginary})^2$$

The magnitude of Z is then utilized to solve for resistance denoted by,

$$\frac{1}{Z} = \frac{1}{R} + \frac{1}{\acute{\imath}\omega C}$$

Where the resistance corresponds to the bulk, grain-boundary, and electrode resistances. The relationship between resistance and conductivity can be denoted as,

$$R = \rho\frac{l}{A} = \frac{1}{\sigma}\frac{l}{A}$$

For a sample of l, thickness, and A, area. The conductivity, σ, is measured in Siemens per centimeter (S/cm) for small pellets.

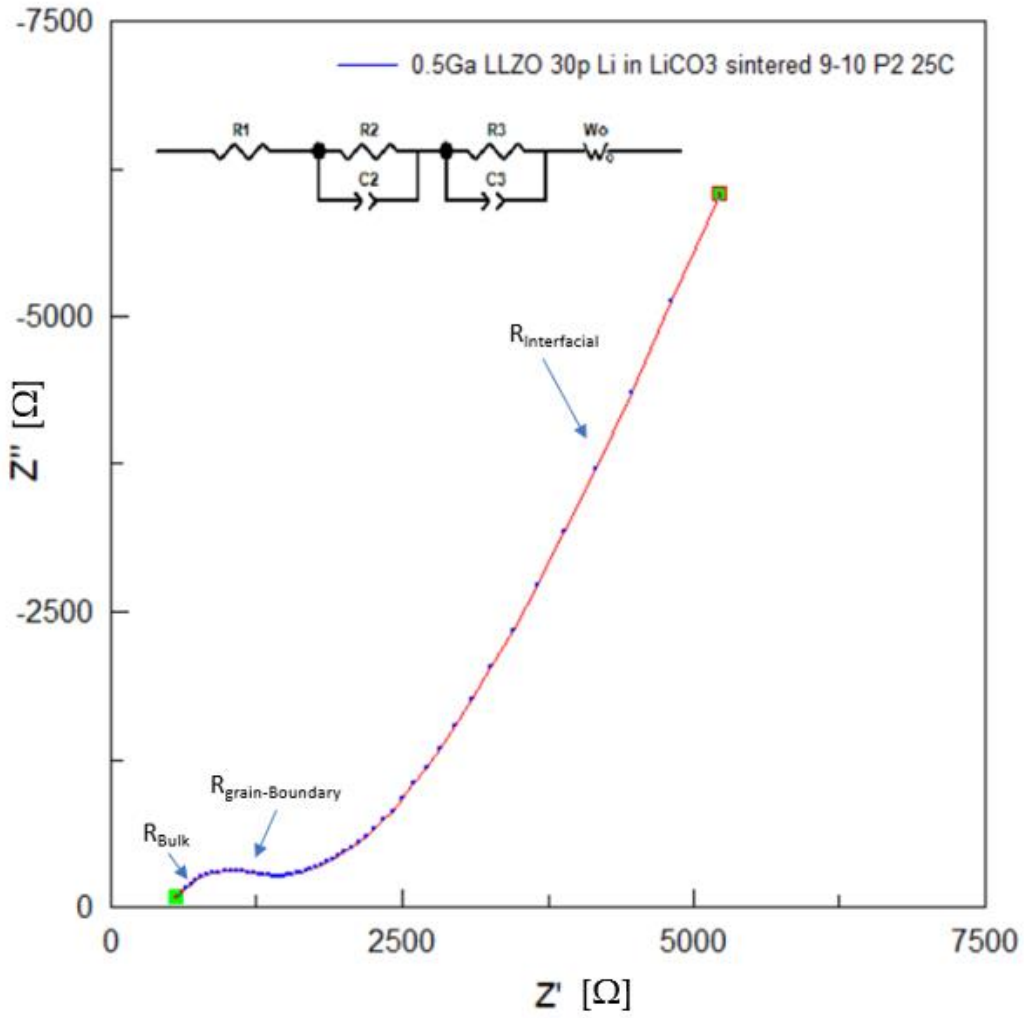

Figure 5-2 Nyquist plot of imaginary and real Z values

Figure 5-2 displays an impedance plot of 0.5 Ga-LLZO with thirty percent excess lithium and boating at room temperature. The impedance plot corresponds with the equivalent circuit shown at the top of the plot. The semi-circle at the beginning of this impedance plot is actually two semi-circles together with a small dip connecting them. These two semi-circles represent the bulk resistance and the grain-broundary resistance

as labeled in the plot though they often form into one semicircle. The semicircle is also attributed to the high frequency conductivity. The bulk resistance refers to the bulk contribution of the pellet, while the grain-boundary resistance is due to the grains and the boundaries separating them. The ‘tail’ or dispersive line of the impedance plot is attributed to the interfacial resistance and is responsible for the low frequency conductivity. This is the resistance caused by the silver paste on the pellets and the electrodes. The tail also contains what is known as the warburg impedance, W_O, denoted in the equivalence circuit in Figure 5-2. The shape of Nyquist plot is similar to that found in literature. [21]

5.2 Conductivity Results

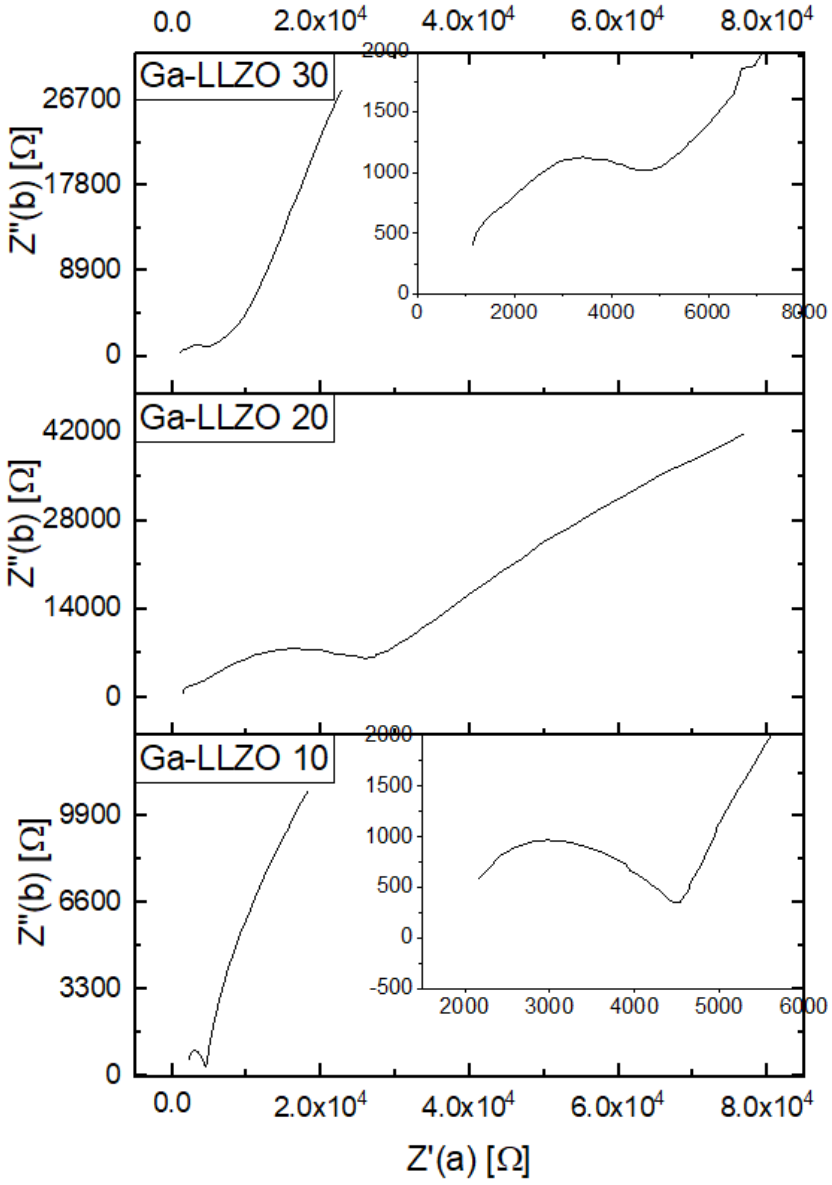

Figure 5-3 Impedance plot of Ga-LLZO samples at room-temperature

Figure 5-3 shows the impedance plots of three Ga-LLZO samples with ten, twenty, and thirty percent excess lithium precursors that were all boated. The Ga-LLZO with 30% excess lithium has two semicircles before its tail indicating more defined bulk resistance and grain-boundary resistance. Ga-LLZO with 20% excess lithium displays the

two semicircles more morphed together indicating less bulk and grain-boundary resistances. The Ga-LLZO with 10% excess lithium has two very small morphed semicircles indicating bulk and grain-boundary resistances indicating a higher conductivity and lower resistance than the other two doped samples.

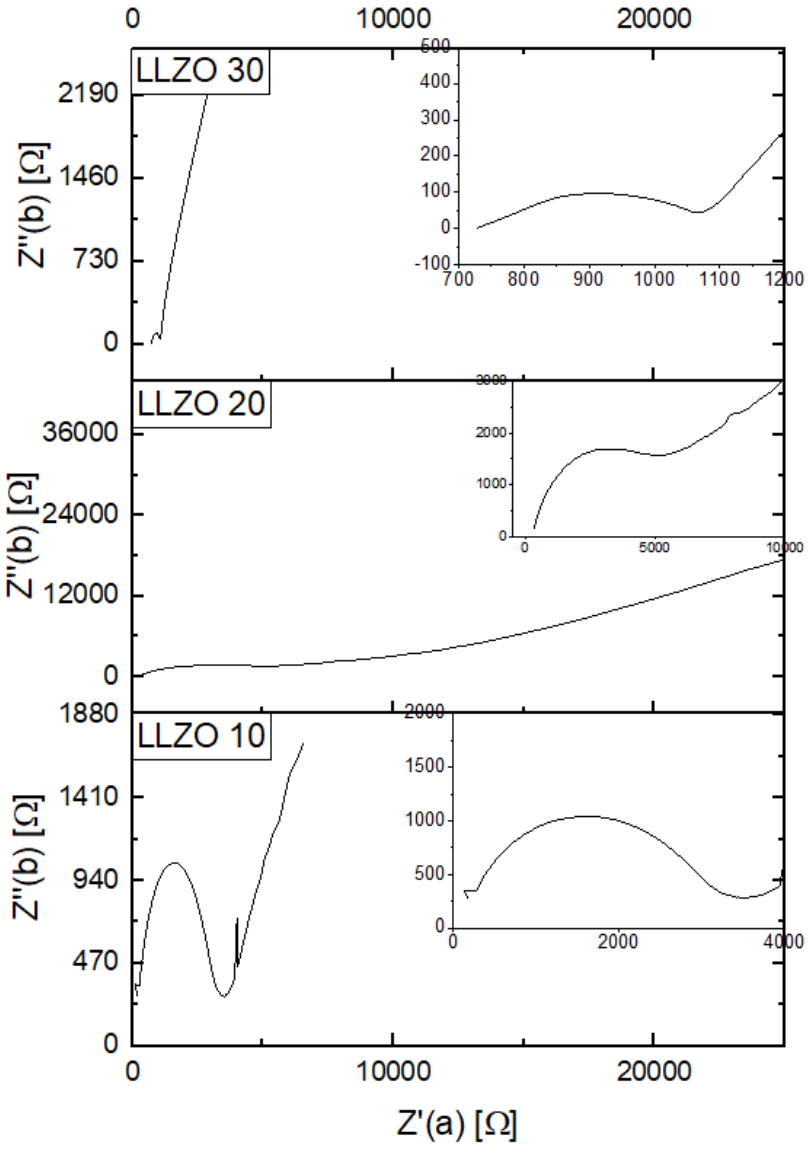

Figure 5-4 Undoped LLZO samples impedance plot

Figure 5-4 displays the undoped LLZO samples with different amounts of excess Li, all samples were boated. In the pure LLZO data set, LLZO 30 had the smallest semi circle indicating a low bulk and grain boundary impedance. LLZO 10 has a larger impedance than LLZO 30 but much smaller impedance than the LLZO 20. It can also be noted that Ga-LLZO 20 and LLZO 20 both had far larger Z'(a) ranges than their comparative samples. LLZO with 20% excess Li shows a drawn out semi circle and tail with the largest impedance values of the pure LLZO samples. While LLZO with 30% excess Li has a small bulk resistance before tailing at the end. LLZO with 10% excess Li shows a uniform semicircle and tail with a discrepancy at about 4000 Ω. The discrepancy shows a sudden jump in impedance that does not align with the rest of the data indicating it is an outlier and should be ignored. Figure 5-3 and Figure 5-4 suggest that too much excess lithium can lead to more resistance and less conductivity and that in particular twenty percent excess leads to a higher impedance than ten percent excess lithium. The figures also suggest that 10% excess lithium with boating is the proper amount of excess lithium to compensate for lithium loss.

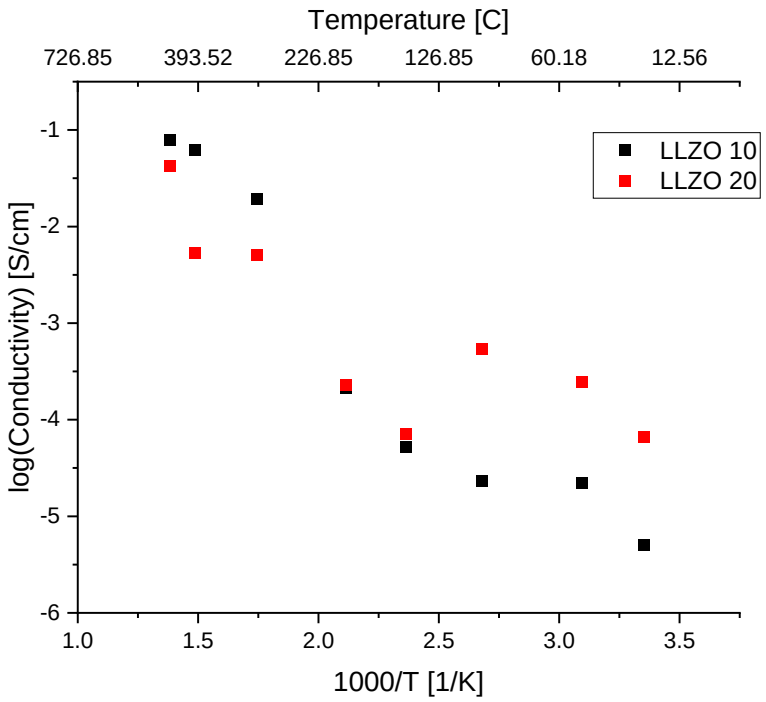

Figure 5-5 Arrhenius plot of pure LLZO samples

Arrhenius plots graphs conductivity data by log of the conductivity on the Y-axis and 1000/Temperature on the X-axis. The temperatures tested range from room temperature, 25℃, to 450℃. This temperature was chosen to test how the solid electrolyte holds up at room temperature as well as high temperatures that may occur during a runaway battery accident type of scenario. Higher temperatures are also of interest to look at due to the transition temperature at about 200℃ of pure LLZO from tetragonal to cubic. [60] A typical arrhenius plot should show a downward trend. Figure 5-5 displays the arrhenius plot of the pure LLZO samples with 10 and 20% excess Li precursor. Both samples show similar results with poor conductivity of ~10^{-5} a full order of magnitude lower than cubic LLZO. The pure LLZO samples have this poor conductivity because they have a tetragonal crystal system and lower densities than Ga-

LLZO samples. At 2 K^{-1}, corresponds to 227˚C, there is a jump from the data points of both samples from the data points having a steeper slope above 227℃ and a lower slope at temperatures below 227℃ signifying a jump in conductivity. This is around the temperature where a reversible phase transition occurs from tetragonal pure LLZO to cubic pure LLZO, about 200℃. The jump in conductivity shows that above the transition temperature the pure LLZO samples will have a higher conductivity because they are likely a cubic crystal system rather than tetragonal. [29]

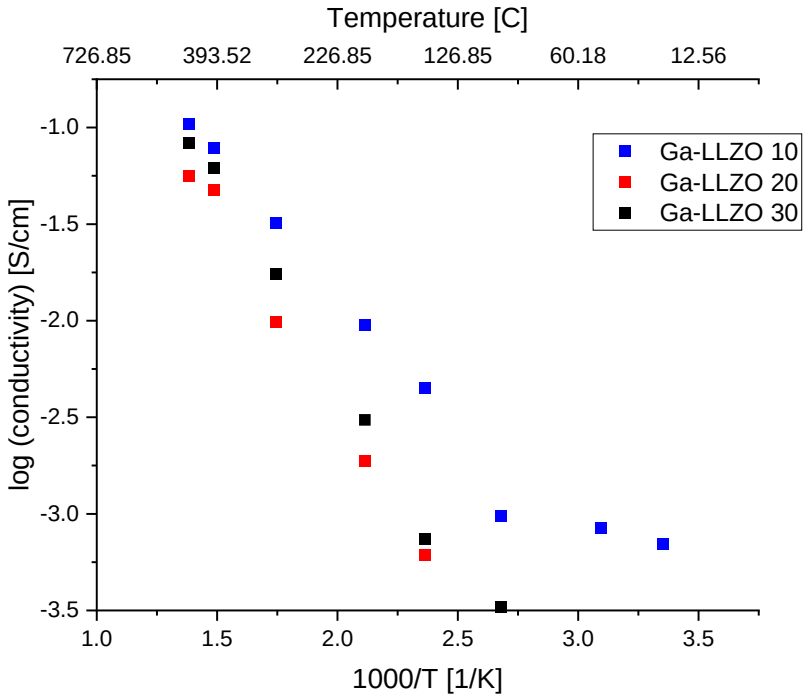

Figure 5-6 Arrhenius plots of Ga-LLZO samples

Figure 5-6 displays the Arrhenius plot of the Ga-LLZO samples with ten, twenty, and thirty percent excess Li precursor. The doped samples do not show a sudden jump in conductivity at 227˚C like the pure LLZO samples did, instead the Ga-LLZO samples show uniform downward trends along their respective trendlines. This uniform

downward trend is because the doped samples have a stabilized cubic structure consistently with every temperature in the range while the pure LLZO samples only exhibited cubic structures at higher temperatures. [60] All the Ga-LLZO samples have results in the same magnitude of ~10^{-4} which is a good range for solid-state electrolytes. The highest conductivity results were found with the 0.5 Ga-LLZO with ten percent excess Li precursor. This corresponds with its microstructure results as it had the highest relative density and largest grains.

Sample Name	Conductivity (STP) [S/cm]	Activation Energy [eV]	Average Grain Size [μm]	Relative Density
LLZO 10% excess Li	2.3×10^{-5}	0.482	1.523	82.09%
LLZO 20% excess Li	5.45×10^{-5}	0.336	2.110	80.86%
LLZO 30% excess Li	3.44×10^{-5}	0.321	2.107	80.19%
0.5 Ga LLZO 10% excess Li	9.78×10^{-4}	0.234	2.450	88.31%
0.5 Ga LLZO 20% excess Li	2.72×10^{-4}	0.447	1.152	84.68%
0.5 Ga LLZO 30% excess Li	3.30×10^{-4}	0.309	1.864	83.13%
$Li_{6.75}La_3Zr_{1.75}Ta_{0.25}O_{12}$ with 8wt% excess Li_2O [27]	2.70×10^{-4}	0.39		97.3%

Al-LLZO ($(La_3Zr_2Al_{0.25})CO_3/OH$) [61]	3.32×10^{-4}	0.32		96.50%
$Ga_{0.42}Li6.64La_3Zr_{2.02}O_{12}$ [21]	5.70×10^{-4}	0.26		92.80%
($Li_{6.4}Ga_{0.2}La_3Zr_2O_{12}$) [23]	1.09×10^{-3}	0.22		95.4%

Table 5-1 Experimental results of LLZO samples

Table 5-1 displays the conductivity, activation energy, average grain size, and relative density for each sample type and reference data. The activation energy and conductivity are influenced by grain size and relative density. Table 5-1 reveals that 0.5 Ga-LLZO with ten percent excess lithium precursor has the highest conductivity, lowest activation energy, largest grain size, and highest relative density. This means this pellet has a crystal system and microstructure to support a high conductivity which is ideal for a solid-state electrolyte.

The reference data show higher density than any of the experimental data in this project. However, despite the larger than 90% densities, they mostly show higher activation energies and lower conductivities than the experimental Ga-LLZO with 10% excess lithium. This shows that conductivity and density may not be as dependent on each other as expected. While higher density electrolytes tend to have higher conductivity, it is not the only characteristic to influence ionic conductivity. The only reference data with a higher activation energy than the experimental Ga-LLZO with 10% excess Li is the $Li_{6.4}Ga_{0.2}La_3Zr_2O_{12}$ which utilized sintering temperature to manipulate

the lithium concentration in the LLZO rather than focusing on adding additional lithium. [23] This is something to consider incorporating with excess lithium for future work.

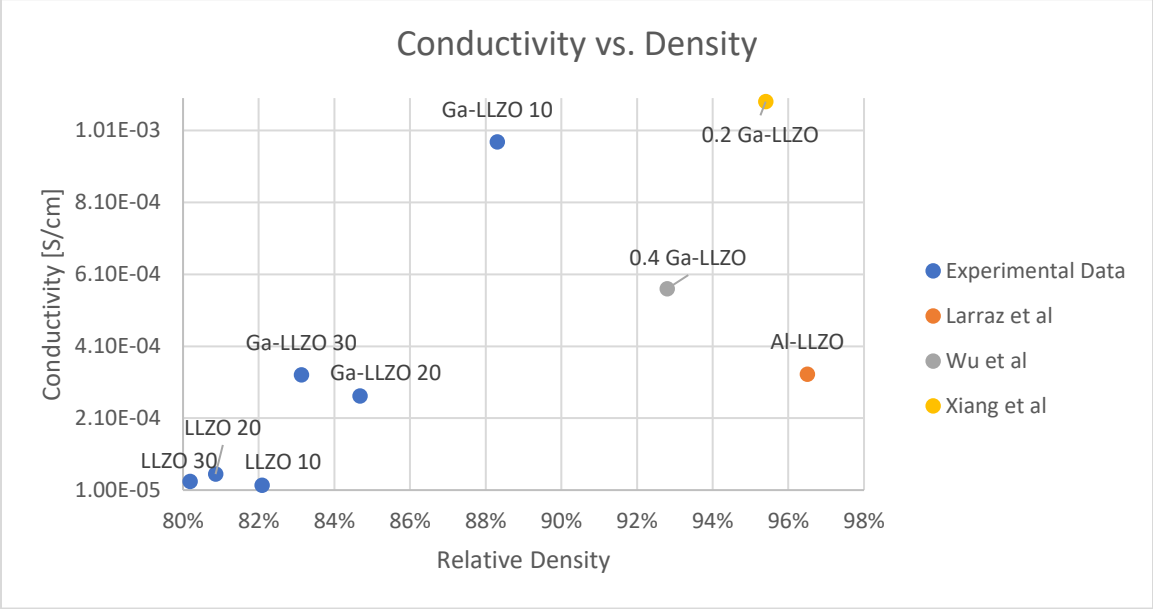

Figure 5-7 Plot of conductivity vs. density of experimental data and reference data [21], [23], [29]

Figure 5-7 displays the plot of conductivity in S/cm by relative density for various compositions of LLZO. The blue points are experimental data and the shorthand names for the compositions are above the corresponding data point.

The experimental data shows a trend as relative density increases the conductivity increases which is to be expected. LLZO compositions and Ga-LLZO compositions both show their thirty percent excess composition as the lowest density and conductivity, 20 percent excess being in the middle, and 10 percent excess as the highest density and conductivity. This shows that ten percent excess lithium regardless of the presence of a dopant is the optimal amount of excess lithium precursor to add. If there is too much lithium it can take up too many vacancies lowering the overall density and conductivity.

It can also be seen that every doped composition, experimental and reference, have conductivities larger than $2.1x10^{-4}$ S/cm while all the experimental undoped LLZO samples have conductivities lower than that.

The reference data shows relative densities superior to the experimental data, however the experimental Ga-LLZO with ten percent excess lithium has the highest conductivity compared to all the reference data points. The 0.4 Ga-LLZO is the closest compositionally to the experimental 0.5 Ga-LLZO samples, but the reference is still 0.0004 S/cm lower than the Ga-LLZO 10 sample. [21] The aluminum LLZO reference point has the highest relative density but a lower conductivity than many of the other reference points. [29]

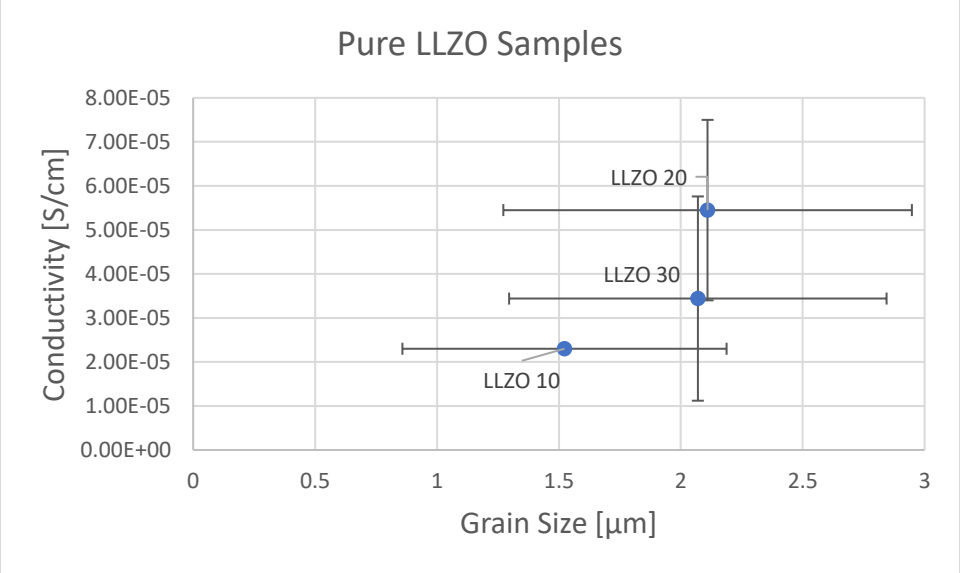

Figure 5-8 Plot of grain size vs. conductivity for pure LLZO samples with different amount of excess lithium precursor

Figure 5-8 displays the conductivity by grain size for pure LLZO with either ten, twenty, or thirty percent excess lithium precursor as labeled in the plot. The error bars are calculated using a population standard deviation of all grain sizes and conductivities for

each type of sample, about 50 grain size measurements and 3 conductivity measurements per sample composition. All pure LLZO compositions are between 1.5 and 2.5 microns. The conductivities between the different samples are roughly comparable in the ~10^{-5} S/cm range, however this is a magnitude below what most doped LLZO samples in literature show. [16], [19], [62] While the amount of excess lithium precursor does not show a correlation in Figure 5-8, there is a correlation between larger grain size and higher conductivity which is shown in literature as well. [57], [63] All of the samples are similar in grain size and conductivity values but as the grain size increases, the conductivity increases as well. The error bars also reveal that as the grain sizes get larger, the standard deviation of grain size does as well. LLZO 10 has the smallest grain size error bar, and while it has the lowest conductivity of the pure LLZO samples, it has a conductivity error of only 2.96×10^{-7} which is two magnitudes smaller than the other two pure LLZO samples.

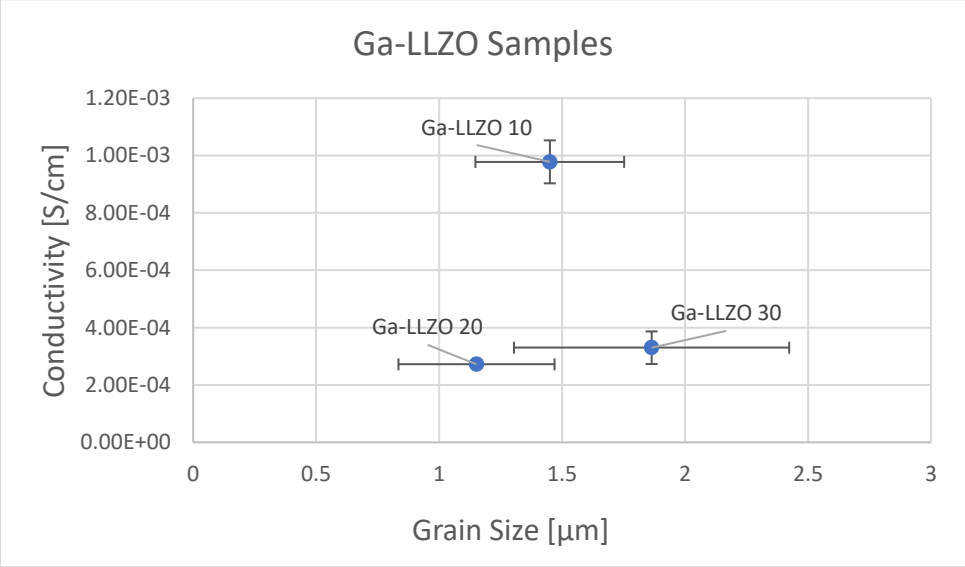

Figure 5-9 Plot of grain size vs. conductivity for gallium doped LLZO samples with different amount of excess lithium precursor

Figure 5-9 displays a grain size against conductivity plot for gallium doped LLZO samples. All the Ga-LLZO samples had conductivities in the ~10^{-4} S/cm magnitude while in Figure 5-8 the pure LLZO samples only had conductivities in the ~10^{-5} S/cm magnitude. While the Ga-LLZO samples have significantly higher conductivity than the pure samples, the grain sizes of the Ga-LLZO samples are still between 1-2 microns, like the pure LLZO grain sizes. This shows the benefit of the dopant and the cubic structure of Ga-LLZO compared to the tetragonal pure LLZO samples. The dopant along with the excess lithium achieves a cubic structure close to the targeted composition, which in turn produces a highly conductive solid electrolyte. The doped samples also show smaller errors for conductivity than the pure LLZO samples, showing that the cubic structure produces more consistent results as well. Ga-LLZO 10 has the highest conductivity out of all the samples tested in this research, while maintaining the smallest errors to show it performs well and consistently.

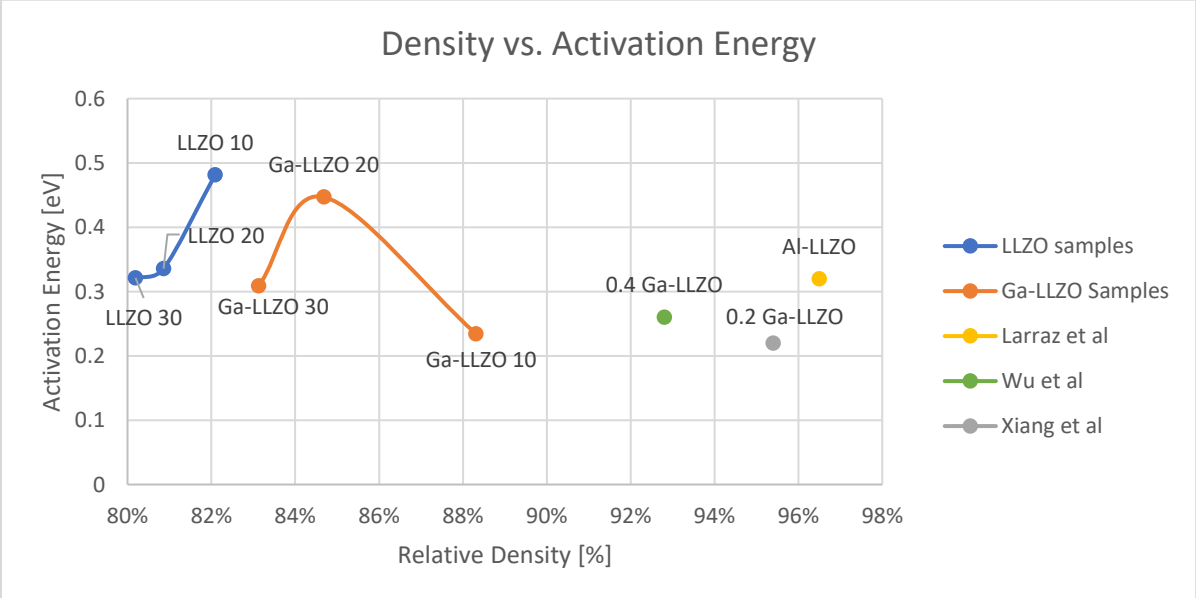

Figure 5-10 Plot of relative density vs. activation energy [21], [23], [29]

Figure 5-10 displays the relative densities of samples against their activation energies. The lines show the LLZO and Ga-LLZO experimental samples with the amount of excess lithium precursor above each data point for reference. The green [21], yellow [29], and gray [23] data points are from their respective literature to provide references against the experimental data. In the experimental data with undoped LLZO samples as excess lithium amount decreases the activation energy and relative density increases. However, the Ga-LLZO samples show that as excess lithium amount decreases the density increases but the activation energy fluctuates. For Ga-LLZO samples the twenty percent excess lithium sample had the largest activation energy while the ten percent excess lithium sample had the lowest activation energy.

The reference data in Figure 5-10 shows that the Al-LLZO, 0.4 Ga-LLZO, and 0.2 Ga-LLZO have higher density than the experimental data, however their activation energies were around the same as the experimental data. The lowest activation energy out of the experimental data and reference data was 0.5 Ga-LLZO with 10% excess lithium precursor. This sample shows a high density and the lowest activation energy across the data making it a formidable solid-state electrolyte.

Overall, the experimental Ga-LLZO samples had comparable conductivities in the same order as most of the literature data found, ~10^{-4} S/cm. This shows that the experimental data has had similar success to other literature. While the experimental data is not necessarily superior to other methods solid electrolytes it displays that excess lithium and the boating technique is a competitive method to what is currently being investigated.

The conductivity data shows that adding excess lithium can help the conductivity, but too much excess lithium can then damper the conductivity. Ten percent excess lithium precursor was proven to be the ideal amount for conductivity testing as the Ga-LLZO 10 had the highest room-temperature conductivity out of all experimental data. Ga-LLZO 20 and Ga-LLZO 30 were prepared the same way as the Ga-LLZO 10 except for additional excess lithium. The higher excess lithium content resulted in poorer conductivity likely due to not enough lithium vacancies for conductivity flow while the Ga-LLZO has the ideal amount of lithium to reach the targeted stoichiometry and leave the ideal amount of lithium vacancies for ion flow.

CHAPTER SIX

CHAPTER SIX

CONCLUSIONS AND FUTURE WORK

Solid-state electrolytes require additional development in order to accelerate entry into the next generation of battery systems. The main difficulties with solid state electrolytes are the lower conductivity and lithium loss as compared to state-of-the-art organic liquid electrolytes. LLZO used as a solid-state electrolyte retain a cubic structure in order to have a competitive conductivity in comparison with liquid electrolytes. In order to attain this cubic structure, it is important to look at getting the targeted composition to achieve a cubic structure. This means making sure there is not too much lithium loss. This work investigated the most efficient ways to attain cubic LLZO with a high conductivity. Specifically, this research looked at how adding excess lithium can achieve a cubic structure with high density and conductivity.

6.1 Structures

The lattice structure of LLZO must be cubic in order to have a high conductivity. The cubic lattice structure was achieved using a dopant and excess lithium in this research. The aluminum dopant used resulted in broken samples after sintering and a low relative density. The gallium dopant used in LLZO resulted in a cubic system, high relative density, and high conductivity. All gallium doped LLZO samples resulted in cubic lattice structures based on X-Ray diffraction results. While the boating technique for excess lithium helps prevent lithium from evaporating and maintaining the targeted composition, it is not involved until after calcining when the cubic structure is reached. Boating helps to prevent more lithium from evaporating during the sintering process, it is

important to maintain the targeted composition throughout calcining and sintering. The excess lithium precursors was added in order to reach the targeted composition and structure, but there must be an appropriate amount of lithium in the sample so that there are exactly three lithium vacancies in the structure, one that will be filled by the dopant, gallium, and two that remain as vacancies in the cubic structure. Ga-LLZO with ten percent excess lithium precursor showed a stable cubic structure and had the highest relative density. Along with the dopant, and adequate amount of lithium must be in the sample in order to reach the targeted composition after sintering while maintaining a cubic structure.

6.2 Microstructures

The ultimate microstructure of LLZO is an important parameter for a useful solid electrolyte. The sample needs to have high density, low porosity, and a uniform large grain size and shape. These characteristics of the microstructure affect how effective the sample is as a solid-state electrolyte. The boating technique for excess lithium proved to be useful as samples utilizing the boating technique exhibited the highest densities. The boated samples also showed adequate lithium content compared to the samples that did not utilize the boating technique. The Ga-LLZO with ten percent excess lithium precursor with boating showed the most ideal characteristics. This sample exhibited actual compositions close to the targeted composition based on ICPMS and EDX data. Other samples were close to their targeted compositions however, the twenty and thirty weight percent excess samples showed actual compositions that were further off from targeted than the ten weight percent samples were. It has a high relative density as well as large

grains with relatively uniformly shaped grains. While Ga-LLZO with ten percent excess lithium has smaller grains than the Ga-LLZO with thirty percent excess lithium, there is only a 0.4 μm difference which is not considered significant. Ga-LLZO with ten percent excess lithium also had the lowest standard deviation in grain size of all samples meaning it has the most consistent grain size and shape. Overall, Ga-LLZO with ten percent excess lithium precursor and the boating technique had the most ideal microstructure out of all experimental samples.

6.3 Conductivity Results

Solid state electrolytes need to have high ionic conductivity for them to be considered possible replacements to liquid in conventional batteries. The undoped LLZO samples all have tetragonal lattice structures which displayed poor conductivity results on the order of ~10^{-5} S/cm. This is to be expected as literature has shown us that in general tetragonal LLZO does not have a high ionic conductivity and therefore are not useful as solid state electrolytes. [18], [28] In comparison, doped LLZO samples all attained a cubic lattice system and had conductivities in the magnitude of ~10^{-4} S/cm which is on the same order of magnitude as most solid-state electrolytes. Ga-LLZO with ten percent excess lithium precursor had the highest conductivity of 9.78 x 10^{-4} S/cm as well as the lowest activation energy of 0.234 eV. This shows that due to Ga-LLZO with ten percent excess lithium sample's structure and microstructure characteristics it was able to have the highest conductivity and therefore the most useful sample for solid state electrolytes.

6.4 Future Work

This project has attempted to improve the preparation methods for LLZO solid-state electrolytes by controlling the amount of excess Li. The research can continue by investigating further how the lithium content supports the cubic stable lattice, while facilitating a dense and large grained microstructure. This research reviewed how lithium content effects LLZO but future research can change the control groups to better analyze the ideal LLZO electrolyte. It would also be beneficial to look closer at the boating technique and how to maximize its use, either by finding a way to add more to the crucible and how that will change the structure and microstructure. The lithium content should be altered in more ways to see how it affects the elemental contents, structure, microstructure, and conductivity, particularly it would be interesting to see how five and fifteen percent excess lithium precursor differ from the ten percent excess precursor in this research. Another path for further research is making two or three gram sample pellets with a 15 mm die to see how thicker samples affect conductivity. If an easy and ideal method for making LLZO is found that produces a high conductivity that challenges a liquid electrolyte than the ideal sample will have been found. The research for solid electrolytes can continue to improve as new methods are attempted based off this research and other literature.

REFERENCES

[1] M. Development, “All-solid-state batteries,” vol. 11, 1984.

[2] L. Kong, C. Li, J. Jiang, and M. G. Pecht, “Li-ion battery fire hazards and safety strategies,” *Energies*, vol. 11, no. 9, p. 2191, 2018.

[3] D. Lisbona and T. Snee, “A review of hazards associated with primary lithium and lithium-ion batteries,” *Process Saf. Environ. Prot.*, vol. 89, no. 6, pp. 434–442, 2011.

[4] K. Kerman, A. Luntz, V. Viswanathan, Y.-M. Chiang, and Z. Chen, “Review—Practical Challenges Hindering the Development of Solid State Li Ion Batteries,” *J. Electrochem. Soc.*, vol. 164, no. 7, pp. A1731–A1744, 2017.

[5] Q. Liu *et al.*, “Challenges and perspectives of garnet solid electrolytes for all solid-state lithium batteries,” *J. Power Sources*, vol. 389, no. April, pp. 120–134, 2018.

[6] K. Liu, J. T. Ma, and C. A. Wang, “Excess lithium salt functions more than compensating for lithium loss when synthesizing Li6.5La3Ta0.5Zr 1.5O12 in alumina crucible,” *J. Power Sources*, vol. 260, pp. 109–114, 2014.

[7] S. C. Levy and P. Bro, *Battery hazards and accident prevention*. Springer Science & Business Media, 1994.

[8] N. Williard, W. He, C. Hendricks, and M. Pecht, “Lessons learned from the 787 dreamliner issue on Lithium-Ion Battery reliability,” *Energies*, vol. 6, no. 9, pp. 4682–4695, 2013.

[9] M. J. Loveridge *et al.*, “Looking deeper into the galaxy (Note 7),” *Batteries*, vol. 4, no. 1, pp. 1–11, 2018.

[10] A. Manthiram, X. Yu, and S. Wang, “Lithium battery chemistries enabled by solid-state electrolytes,” *Nat. Rev. Mater.*, vol. 2, no. 4, pp. 1–16, 2017.

[11] J. Wolfenstine, J. L. Allen, J. Sakamoto, D. J. Siegel, and H. Choe, “Mechanical behavior of Li-ion-conducting crystalline oxide-based solid electrolytes: a brief review,” *Ionics (Kiel).*, vol. 24, no. 5, pp. 1271–1276, May 2018.

[12] K. Liu, J. T. Ma, and C. A. Wang, “Excess lithium salt functions more than compensating for lithium loss when synthesizing Li6.5La3Ta0.5Zr 1.5O12 in alumina crucible,” *J. Power Sources*, 2014.

[13] C. Li, Y. Liu, J. He, and K. S. Brinkman, “Ga-substituted Li7La3Zr2O12: An investigation based on grain coarsening in garnet-type lithium ion conductors,” *J. Alloys Compd.*, vol. 695, pp. 3744–3752, 2017.

[14] S. Yu *et al.*, “Elastic Properties of the Solid Electrolyte Li7La3Zr2O12 (LLZO),” *Chem. Mater.*, vol. 28, no. 1, pp. 197–206, 2016.

[15] Y. Jin and P. J. McGinn, “Al-doped Li 7La 3Zr 2O 12 synthesized by a polymerized complex method,” *J. Power Sources*, 2011.

[16] Y. Li *et al.*, “W-Doped Li7La3Zr2O12 Ceramic Electrolytes for Solid State Li-ion Batteries,” *Electrochim. Acta*, 2015.

[17] L. J. Miara, W. D. Richards, Y. E. Wang, and G. Ceder, “First-Principles Studies on Cation Dopants and Electrolyte|Cathode Interphases for Lithium Garnets,” *Chem. Mater.*, vol. 27, no. 11, pp. 4040–4047, 2015.

[18] T. Thompson *et al.*, “Tetragonal vs. cubic phase stability in Al-free Ta doped Li 7La3Zr2O12 (LLZO),” *J. Mater. Chem. A*, vol. 2, no. 33, pp. 13431–13436, 2014.
[19] S. Song *et al.*, “Gd-doped Li7La3Zr2O12 garnet-type solid electrolytes for all-solid-state Li-Ion batteries,” *Electrochim. Acta*, vol. 270, pp. 501–508, 2018.
[20] H. El Shinawi and J. Janek, “Stabilization of cubic lithium-stuffed garnets of the type ‘li 7La3Zr2O12’ by addition of gallium,” *J. Power Sources*, vol. 225, pp. 13–19, 2013.
[21] J. F. Wu *et al.*, “Gallium-doped Li7La3Zr2O12 garnet-type electrolytes with high lithium-ion conductivity,” *ACS Appl. Mater. Interfaces*, vol. 9, no. 2, pp. 1542–1552, 2017.
[22] S. Aktaş *et al.*, “Study of the local structure and electrical properties of gallium substituted LLZO electrolyte materials,” *J. Alloys Compd.*, vol. 792, pp. 279–285, 2019.
[23] X. Xiang, F. Chen, Q. Shen, L. Zhang, and C. Chen, “Effect of the lithium ion concentration on the lithium ion conductivity of Ga-doped LLZO,” *Mater. Res. Express*, vol. 6, no. 8, 2019.
[24] M. Wang and J. Sakamoto, “Correlating the interface resistance and surface adhesion of the Li metal-solid electrolyte interface,” 2017.
[25] W. Hou, X. Guo, X. Shen, K. Amine, H. Yu, and J. Lu, “Solid electrolytes and interfaces in all-solid-state sodium batteries: Progress and perspective,” *Nano Energy*, vol. 52, no. July, pp. 279–291, 2018.
[26] S. H. Yang *et al.*, “Ionic conductivity of Ga-doped LLZO prepared using Couette–Taylor reactor for all-solid lithium batteries,” *J. Ind. Eng. Chem.*, vol. 56, pp. 422–427, 2017.
[27] Y. Li, Y. Cao, and X. Guo, “Influence of lithium oxide additives on densification and ionic conductivity of garnet-type Li6.75La3Zr 1.75Ta0.25O12 solid electrolytes,” *Solid State Ionics*, 2013.
[28] J. Wolfenstine, E. Rangasamy, J. L. Allen, and J. Sakamoto, “High conductivity of dense tetragonal Li 7La 3Zr 2O 12,” *J. Power Sources*, vol. 208, pp. 193–196, Jun. 2012.
[29] G. Larraz, A. Orera, and M. L. Sanjuán, “Cubic phases of garnet-type Li7La3Zr 2O12: The role of hydration,” *J. Mater. Chem. A*, vol. 1, no. 37, pp. 11419–11428, 2013.
[30] C. A. Geiger *et al.*, “Crystal chemistry and stability of ‘Li7La 3Zr2O12’ garnet: A fast lithium-ion conductor,” *Inorg. Chem.*, vol. 50, no. 3, pp. 1089–1097, 2011.
[31] J. D. Percival, “Synthesis and Characterisation of Novel Lithium Ion Containing Garnet-related Materials for Potential Lithium Ion Battery Applications,” 2009.
[32] S. Afyon, F. Krumeich, J. L. M Rupp, and G. Li, “A shortcut to garnet-type fast Li-ion conductors for all-solid state batteries †,” 2015.
[33] S. Ramakumar, C. Deviannapoorani, L. Dhivya, L. S. Shankar, and R. Murugan, “Lithium garnets: Synthesis, structure, Li+ conductivity, Li+ dynamics and applications,” *Progress in Materials Science*. 2017.
[34] A. Equipment, N. Publishing, P. Examiner, C. E. Church, A. Examiner, and K. Suchecki, “(12) United States Patent,” vol. 2, no. 12, 2006.

[35] B. D. Cullity, *Elements of X-Ray Diffraction*. 1956.
[36] L. J. Poppe, V. F. Paskevich, J. C. Hathaway, and D. S. Blackwood, "A Laboratory Manual For X-Ray Powder Diffraction," *US Geol. Surv. Open-File Rep.*, vol. 1.041, pp. 1–88, 2001.
[37] H. Schatten, "Scanning Electron Microscopy for the Life Sciences," in *SCANNING ELECTRON MICROSCOPY FOR THE LIFE SCIENCES*, THE PITT BUILDING, TRUMPINGTON ST, CAMBRIDGE CB2 1RP, CAMBS, ENGLAND: CAMBRIDGE UNIV PRESS, 2013, pp. 1–261.
[38] H. J. Leamy, "Charge collection scanning electron microscopy," *J. Appl. Phys.*, vol. 53, no. 6, 1982.
[39] P. Books, S. With, and T. Electron, "Scanning And Transmission Electron Microscopy An Introduction sc an ni ng an d tr an Microscopy An Introduction Are Listed Below : sm iss io ec tr on m ic ro sc y in tr od uc tio n sc ni ng an d tr an sm io ec tr on m ic ro in tr od uc tio n."
[40] D. Klenov, B. Freitag, H. von Harrach, A. D'Alfonso, and L. Allen, "Chemical Mapping at the Atomic Level using Energy Dispersive X-ray Spectroscopy," *Microsc. Microanal.*, vol. 17, no. S2, pp. 598–599, 2011.
[41] Kazmiruk, V, Ed., "Scanning Electron Microscopy," in *SCANNING ELECTRON MICROSCOPY*, JANEZA TRDINE9, RIJEKA, 51000, CROATIA: INTECHOPEN, 2012, pp. 1–830.
[42] B. D. Forbes *et al.*, "Contribution of thermally scattered electrons to atomic resolution elemental maps," *Phys. Rev. B - Condens. Matter Mater. Phys.*, vol. 86, no. 2, Jul. 2012.
[43] J. I. Goldstein *et al.*, "Special topics in scanning electron microscopy," in *Scanning electron microscopy and x-ray microanalysis*, Springer, 2003, pp. 195–270.
[44] A. Pawlaczyk and M. I. Szynkowska, "Application of ICP-MS for Trace Elemental and Speciation Analysis," in *MASS SPECTROMETRY: AN APPLIED APPROACH, 2ND EDITION*, Smoluch, M and Grasso, G and Suder, P and Silberring, J, Ed. 111 RIVER ST, HOBOKEN, NJ 07030 USA: JOHN WILEY & SONS INC, 2019, pp. 351–361.
[45] C. Iacobucci *et al.*, "Instrumentation," in *MASS SPECTROMETRY: AN APPLIED APPROACH, 2ND EDITION*, Smoluch, M and Grasso, G and Suder, P and Silberring, J, Ed. 111 RIVER ST, HOBOKEN, NJ 07030 USA: JOHN WILEY & SONS INC, 2019, pp. 13–106.
[46] H. J. P. Keighley, F. R. McKim, A. Clark, and M. J. Harrison, "Archimedes' Principle and Flotation," in *Mastering Physics*, London: Macmillan Education UK, 1984, pp. 66–70.
[47] B.-Y. Chang and S.-M. Park, "Electrochemical impedance spectroscopy of composite adhesive joints," *Annu. Rev. Anal. Chem. (Palo Alto. Calif).*, vol. 3, no. 6, pp. 207–229, 2010.
[48] A. Lasia, "Electrochemical Impedance Spectroscopy and its Applications," in *Modern Aspects of Electrochemistry*, B. E. Conway, J. O. Bockris, and R. E. White, Eds. Boston, MA: Springer US, 2002, pp. 143–248.
[49] K. Meier, T. Laino, and A. Curioni, "Solid-state electrolytes: Revealing the

mechanisms of Li-Ion conduction in tetragonal and cubic LLZO by first-principles calculations," *J. Phys. Chem. C*, vol. 118, no. 13, pp. 6668–6679, 2014.
[50] K. Persson, "Materials Data on Li7La3Zr2O12 (SG:142) by Materials Project." 2016.
[51] R. Wagner *et al.*, "Crystal Structure of Garnet-Related Li-Ion Conductor Li7–3xGaxLa3Zr2O12: Fast Li-Ion Conduction Caused by a Different Cubic Modification?," *Chem. Mater.*, vol. 28, no. 6, pp. 1861–1871, 2016.
[52] J. Awaka, A. Takashima, K. Kataoka, N. Kijima, Y. Idemoto, and J. Akimoto, "Crystal structure of fast lithium-ion-conducting cubic Li 7La3Zr2O12," *Chem. Lett.*, vol. 40, no. 1, pp. 60–62, 2011.
[53] K.-H. Zum Gahr, *Microstructure and wear of materials*, vol. 10. Elsevier, 1987.
[54] K.-H. Zum Gahr, "Microstructure and Wear of Materials - ZUM GHAR.pdf," *Elsevier Science Publishers B.V.*, 1987. [Online]. Available: https://books.google.com/books?hl=en&lr=&id=qibApT7zNcYC&oi=fnd&pg=PP1&dq=microstructure&ots=KZaMbLKcQd&sig=0EeWdWLJ7nMLv47XOY7u6wPtVw0#v=onepage&q=microstructure&f=false. [Accessed: 11-Apr-2020].
[55] F. Langer, I. Bardenhagen, J. Glenneberg, and R. Kun, "Microstructure and temperature dependent lithium ion transport of ceramic–polymer composite electrolyte for solid-state lithium ion batteries based on garnet-type Li7La3Zr2O12," *Solid State Ionics*, vol. 291, pp. 8–13, Aug. 2016.
[56] X. Han *et al.*, "Negating interfacial impedance in garnet-based solid-state Li metal batteries," *Nat. Mater.*, vol. 16, no. 5, pp. 572–579, May 2017.
[57] L. Cheng *et al.*, "Effect of microstructure and surface impurity segregation on the electrical and electrochemical properties of dense Al-substituted Li7La 3Zr2O12," *J. Mater. Chem. A*, vol. 2, no. 1, pp. 172–181, Jan. 2014.
[58] R. Halder and S. Bandyopadhyay, "Effect of cation ratio on microstructure and optical absorbance of magnesium aluminate spinel," *Mater. Res. Express*, vol. 7, p. 15065, 2020.
[59] M. E. Orazem and B. Tribollet, *Electrochemical impedance spectroscopy*. John Wiley & Sons, 2017.
[60] N. Bernstein, M. D. Johannes, and K. Hoang, "Origin of the structural phase transition in Li 7La 3Zr 2O 12," *Phys. Rev. Lett.*, vol. 109, no. 20, pp. 1–5, 2012.
[61] Y. Zhang *et al.*, "Preparation of cubic Li7La3Zr2O12 solid electrolyte using a nano-sized core-shell structured precursor," *J. Alloys Compd.*, vol. 644, pp. 793–798, Sep. 2015.
[62] Q. Liu *et al.*, "Challenges and perspectives of garnet solid electrolytes for all solid-state lithium batteries," *J. Power Sources*, vol. 389, no. March, pp. 120–134, 2018.
[63] W. Zhou *et al.*, "Polymer lithium-garnet interphase for an all-solid-state rechargeable battery," *Nano Energy*, vol. 53, pp. 926–931, 2018.